Application of ICP-MS in the optimisation of a new methodology for ^{68}Ga production in a PET dedicated cyclotron

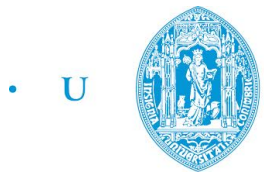

FCTUC FACULDADE DE CIÊNCIAS E TECNOLOGIA
UNIVERSIDADE DE COIMBRA

Magda Filipa Carvalho Silva

Department of Physics

University of Coimbra

Under the supervision of

Dr. Francisco Alves and Dr. José António Paixão, University of Coimbra

A thesis submitted for the degree of

Master in Physics

September, 2016

"We're all stories in the end. Just make it a good one."

- The Doctor

Agradecimentos

Gostaria de agradecer aos professores envolvidos no projecto que sugeriram e me deram as condições necessárias para o desenvolver. Ao Prof. Francisco Alves, ao Prof. José António Paixão e ao Prof. Antero Abrunhosa, obrigada pelo apoio e confiança.

Durante o desenvolvimento do projecto tive a oportunidade de trabalhar com várias pessoas do ICNAS Produção. Agradeço a todos por me integrarem na equipa e se mostrarem disponíveis para me ajudar.

Fica também um obrigada ao Dr. Pedro Silva por todas as horas passadas em frente ao ICP-MS.

Aos meus amigos, todos eles pessoas inacreditáveis e talentosas que fizeram destes últimos anos os melhores (e os piores!) que podiam ser. Um especial obrigada à Adriana e à Susana pela preocupação constante.

Agradeço aos meu pais por tudo o que me ensinaram. Por me darem tempo para perceber quem sou e por acreditarem em mim.

À minha irmã, Eduarda, pelos bons momentos e pelas distrações ao fim do dia. Obrigada por me lembrares a importância de gostar do que se faz.

Ao João, por me fazer continuar quando eu não queria, pela ajuda e infindável paciência. Obrigada por me fazeres tão feliz.

Ainda, à Ângela Guerra, uma das pessoas mais inteligentes e inspiradoras que tive o prazer de conhecer.

Finalmente, agradeço ainda o acesso ao ICP-MS da plataforma
TAIL-UC, financiado pelo programa QREN-Mais Centro ICT_2009_02_012_1890.

Resumo

O objectivo deste trabalho era investigar a existência de contaminação por metais na produção de ^{68}Ga num ciclotrão com alvo líquido. Tais contaminantes apresentam uma química semelhante à do metal $^{68}Ga^{3+}$ e podem ocupar o seu lugar no quelato DOTA, afectando, desta forma, a marcação do ^{68}Ga-DOTA-peptídeo, um análogo da somatostatina, de grande importância para o diagnóstico de tumores endócrinos. Para determinar a presença de contaminantes fez-se uso de uma técnica de ICP-MS. Esta técnica é descrita detalhadamente, uma vez que está a ser usada pela primeira vez para este projecto. Os problemas encontrados durante a utilização do ICP-MS são também largamente discutidos pela sua importância para trabalho futuro.

Amostras de vários passos do processo de produção de ^{68}Ga-DOTA-NOC foram recolhidas e analisadas. Partindo destas amostras foi possível determinar a existência de uma quantidade relevante de ferro na solução de HCl que era usada em vários passos do processo de purificação do ^{68}Ga. Esta conclusão levou-nos a optar por comprar uma nova solução de HCl com um elevado grau de pureza (*ultra-trace*), eliminando assim um importante contaminante da produção. Esta medida ajudou a tornar viável a marcação de ^{68}Ga-DOTA-NOC.

Abstract

The aim of this work was to investigate the existence of metal contamination during the production of ^{68}Ga in a cyclotron with liquid target. Such contaminants present a similar chemistry to metal $^{68}Ga^{3+}$ and can occupy its place in the DOTA chelate, affecting the labelling of ^{68}Ga-DOTA-peptide, an analogous of somatostatin, of great importance in the diagnosis of endocrine tumours. To determine the presence of contaminants an ICP-MS technique was used. This technique is thoroughly described, as it is being used for the first time for this project. The problems faced during the use of the ICP-MS are also greatly discussed for their importance in future work.

Samples of several steps of the ^{68}Ga-DOTA-NOC production process were retrieved and analysed. From these samples it was possible to determine the existence of a relevant quantity of iron in the HCl solution that was used in several steps of the purification process of ^{68}Ga. This conclusion lead us to purchase a new HCl solution with with ultra-trace purity, this way eliminating an important contaminant of the production. This measure helped make viable the labelling of ^{68}Ga-DOTA-NOC.

Keywords: Inductively Coupled Plasma Mass Spectrometry (ICP-MS), Cyclotron, ^{68}Ga, ^{68}Ge/^{68}Ga Generator, ^{68}Ga-DOTA-NOC, Positron Emission Tomography (PET), Metal contaminants, Radiopharmaceuticals.

Contents

List of Figures

List of Tables

List of Acronyms

PET Positron Emission Tomography

FDG 2-deoxy-2-[^{18}F]-fluoro-D-glucose

ICP-MS Inductively Coupled Plasma Mass Spectrometry

PFA Perfluoroalkoxy

RF Radio frequency

SEM Secondary Electron Multiplier

CRC Collision/Reaction Cell

KED Kinetic Energy Discrimination

SPECT Single Photon Emission Computed Tomography

CT Computed Tomography

LOR Line of Response

GHIH Growth Hormone-Inhibiting Hormone

DOTA 1,4,7,10-tetraazacyclododecane-1,4,7,10-tetraacetic acid

NOC [Nal3]-octreotide

TOC (Tyr3)-octreotide

TATE (Tyr3)-octreotate

HEPES 4-(2-hydroxyethyl)-1-piperazineethanesulfonic acid

NET NeuroEndocrine Tumours

STT Somatostatin

STTa SST analogues

IBA Ion Beam Applications

Chapter 1

Introduction

Imaging techniques have drastically changed the way disease is approached. Improvements in morbidity and mortality rates can be associated with early diagnosis and accompanied treatment, both particularly important in the fields of oncology and neurology. Physics has played an enormous role in all this. The development of the cyclotron, back in the 1930s, started the ball rolling and soon after a great arsenal of man-made radioactive isotopes were being investigated. A variety of these radioactive isotopes, or radionuclides, found applications in Nuclear Medicine, a specialty of medical imaging that focus on diagnostic imaging and therapeutic applications. The early applications of radionuclides in this field focused mostly on scintigraphy and respiratory studies [Clark and Buckingham, 1975] [Qaim et al., 1976]. Later, the availability of functional information through the development of emission tomography elevated the value of radionuclides. The possibility of studying, for example, uptake kinetics or metabolic turnover rates of the body was a great achievement in imaging.

Emission tomography comprises two main-techniques, namely, Single Photon Emission Computed Tomography (SPECT) and Positron Emission Tomography (PET) [Wernick and Aarsvold, 2004]. Both techniques rely on the use of radiolabeled imaging agents, suitable for human use, called radiopharmaceuticals. Despite the fact that PET is more expensive, it is agreed that it offers some advantages over SPECT [Bateman, 2012] such as higher spatial-

resolution and higher sensitivity [Rahmim and Zaidi, 2008].

Nowadays identification of functional, and even molecular, abnormalities using PET or the combination PET/CT, which combines the acquisition of functional and anatomical images, is common practice worldwide [Higgins and Pomper, 2011].

Even though the great majority of clinical PET investigation is still performed with the glucose analog 2-deoxy-2-[^{18}F]-fluoro-D-glucose (FDG), interest for specific molecular probes has grown [Sörensen, 2012]. A great deal of research has now been dedicated to finding alternatives to compensate some of the weaknesses of FDG (e.g. failing to differentiate between tumour and inflammation or infection) [Velikyan, 2014]. Among the prominent imaging agents is the metallic, positron emitter, ^{68}Ga. The interest in this radiometal is in great part a result of its nuclear decay characteristics and its accessibility. Furthermore, the ability of ^{68}Ga to label peptides confers faster blood clearance, rapid target identification and tissue penetration and an overall superiority in image quality when compared to other radionuclides [Banerjee and Pomper, 2013]. The most common method for obtaining ^{68}Ga is the use of a generator. Another traditional production method consists in irradiating a solid target in a cyclotron, producing ^{68}Ga via the 68Zn(p,n)68Ga reaction. Through this technique, large activities of 68Ga (with reported yields of about 5?6 GBq/Ah) can be produced. However, there are several disadvantages inherent of the use of solid targets, such as long and sensitive target preparation [**?**], heat dissipation during irradiation, activation of target backing support, contamination from the latter, or post-irradiation target handling including target dissolution process. These drawbacks are so significant that they have been forbidding the spread of this technique despite the attractive amount of activity producible.

To avoid the problems related to the solid target production, it was recently proposed the cyclotron production of ^{68}Ga using liquid targets, and already some solutions were tested [Jensen and Clark, 2011] [Pandey et al., 2014]. At ICNAS, a production method was developed using a zinc nitrate ($^{68}Zn(NO_3)_2$) solution. The intent of this thesis was to investigate and eliminate possible

trace metal contaminants in this process of ^{68}Ga production.

To this end, samples from the varied steps of the process were recovered and analysed by Inductively Coupled Plasma Mass Spectrometry (ICP-MS). ICP-MS is a strong analytical technique, offering extremely low detection limits, that has been used to measure samples of varying composition - from human urine or blood to crude soils or river water [Thomas, 2004].

The determination of trace elements is extremely important in the radiopharmaceutical field. The control of chemical impurities is necessary to assure the safety and efficacy of the radiopharmaceuticals.

This thesis was developed in collaboration with the Institute for Nuclear Sciences Applied to Health (ICNAS) and the Physics Department of the University of Coimbra. In the chapters ahead some background is provided so as to give the reader a clear view of the method employed and the importance and applicability of the radionuclide ^{68}Ga in clinical imaging.

Chapter 2

ICP-MS

Inductively Coupled Plasma Mass Spectrometry (ICP-MS) is a powerful mass spectrometric technique used to identify and quantify trace elements in samples. With clinical research nowadays relying heavily on information on trace-level concentrations there's a need for analytical techniques of the highest sensitivity (ppt level). ICP-MS meets that need, coupling its versatility with the capability to provide accurate information on concentrations and species identity. The superior detection capabilities of ICP-MS led to its early adoption by Geochemical analysis labs, just after its commercialisation in 1983 [Thomas, 2004]. Soon after, many fields - Environmental, Biomedical, Nuclear and Semiconductor - found the technique suitable for their needs. To understand ICP-MS, an overview of its components and an explanation of how they work is necessary. Therefore, in this chapter I proceed to explain its main features.

2.1 ICP-MS general

The technique of ICP-MS couples two well known technologies: inductively coupled plasma and mass spectrometer. Its fundamental principle is the generation of positively charged ions from a high temperature plasma discharge. The masses of these ions are then analysed using mass spectrometry. One of ICP-MS's greatest feats is its large range of operation (8 orders of

magnitude) offering extremely low detection limits (1 pg/mL for many elements) but still enabling quantitation at the high ppm level [Thomas, 2004]. Additionally, a high sample throughput and the ability to obtain isotopic information give this technique many advantages over other elemental analysis techniques [Vandecasteele and Block, 1993].

The scope of elements that can be detected using an ICP-MS can be seen in Figure 2.1.

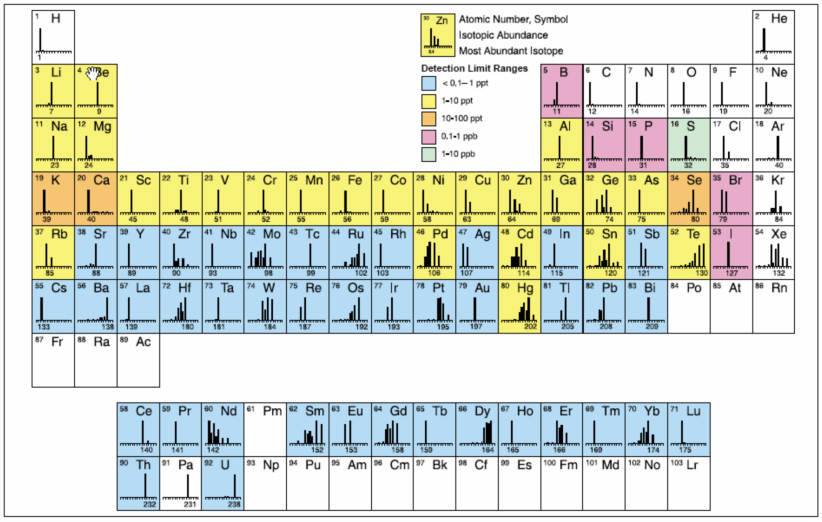

Figure 2.1: Approximate detection capabilities of the quadrupole ICP-MS. Adapted from [Bazilio and Weinrich, 2012].

For better visualisation, this instrument can be divided into its main components:

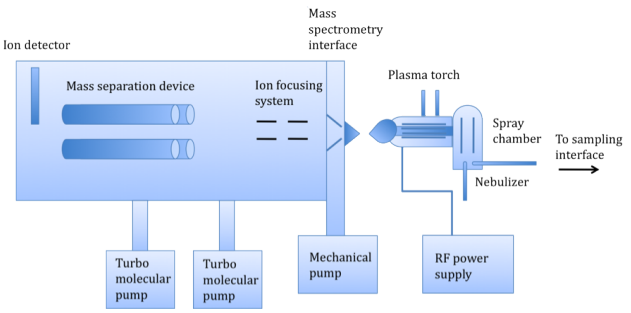

Figure 2.2: Diagram depicting the basic components of an ICP-MS system. Adapted from [Thomas, 2004].

Figure 2.2 shows a schematic overview of a basic ICP-MS instrument, consisting of the sample introduction system, the interface region connected by the ion-focusing system to the mass-separation device and the ion detector, both kept in a vacuum chamber, maintained by turbo molecular pumps.

In the following subchapters a brief description of these systems is provided.

2.1.1 Sample introduction system

Regarded as the most important step in all the process, the sample introduction system holds the fundamental principles of converting a representative part of the liquid sample into a fine droplet aerosol suitable for ionisation in the plasma [Thomas, 2004]. The most common method to achieve this is the use of a nebuliser. The sample introduction system can be seen as two separate events:

1. Aerosol formation

2. Droplet selection

In the first part, the liquid sample is pumped (1mL/min) into the nebuliser[1] using a peristaltic pump, in a way that ensures a constant flow of liquid, be it a sample, standard or blank. Another way to transport the liquid sample to the nebuliser is by creating a pressure drop in the latter causing spontaneous nebulisation.

Once the sample reaches the nebuliser it breaks up into a fine aerosol by the pneumatic action of the gas flow (typically Argon).

After the nebulisation process, the small droplets of aerosol enter the spray chamber[2], where the droplet selection takes place. The spray chamber is made of quartz or Perfluoroalkoxy (PFA) [Thomas, 2004] and provides

[1]The nebuliser can have different designs: concentric, microconcentric, microflow and cross flow. Further information on their characteristics can be found in [Thomas, 2004].

[2]The spray chamber has two typical designs: Scott-type double-pass and Cyclonic spray chamber. The differences between them can be found in [Thomas, 2004].

signal stability and low oxide rates by filtering out the larger aerosol droplets. This way only the smallest droplets are sent off to the plasma source for further analysis. This selection can however also be seen as a weak point of the instrumentation, since only 2-5% of the sample is introduced into the plasma source [Thomas, 2008].

2.1.2 Plasma source and Ion formation

The inductively coupled plasma is used to convert the sample aerosol emerging from the sample introduction system into ions, which are then separated and detected by the mass spectrometer [Houk et al., 1980].

The plasma torch, Radio frequency (RF) coil and power supply compose the plasma source.

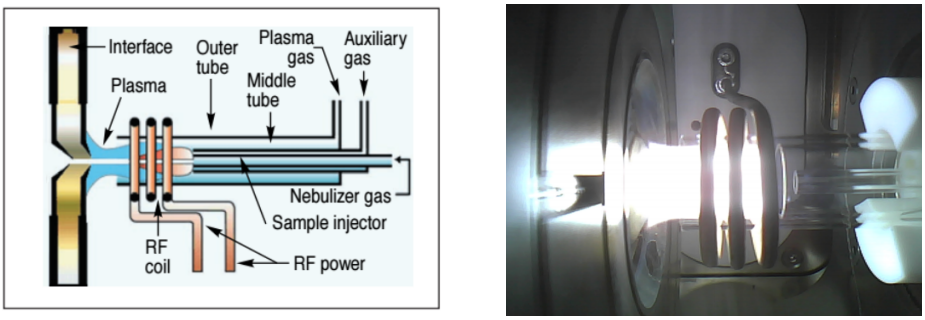

(a) (b)

Figure 2.3: a) Detailed view of plasma torch and RF coil. b) Picture of the plasma chamber.

As can be seen in Figure 2.3, the plasma torch comprises an outer tube, a middle tube and a sample injector.

Between the outer and middle tube, the so called plasma gas flows at a rate of 12-17 L/min, whereas an auxiliary gas, used to optimise the position of the plasma, flows between the middle tube and the sample injector. A third gas, known as the nebuliser gas, transports the sample from the sample introduction system to the torch, where the gas flow physically makes a hole in the centre of the plasma [Thomas, 2004].

The inductively coupled plasma is composed of argon atoms, argon ions

and electrons. This is obtained when the argon flowing in the ICP torch is subject to a high-voltage spark and the electrons are stripped from the argon atoms, resulting in argon ions.

There are different heating zones present in the plasma, as shown in Figure 2.4(a), and each one serves its own purpose in transforming the sample into ions [Thomas, 2008].

In the first step, the droplet of the sample is dried so it becomes solid. After this, the sample passes into the gaseous state by vaporisation, and finally by atomisation it becomes a ground-state atom (Figure 2.4(b)). The sample then proceeds to the analytical zone of the plasma, which is at a temperature of 6000-7000 K. Here the conversion of the atoms into ions occurs, due to collisions with Ar atoms and ions and also energetic electrons. The level of ion formation through this process is related to the ionisation potential of the sample element, with it being easier to ionise when the IP is lower [Thomas, 2008]. When the atoms are ionised they proceed into the interface region.

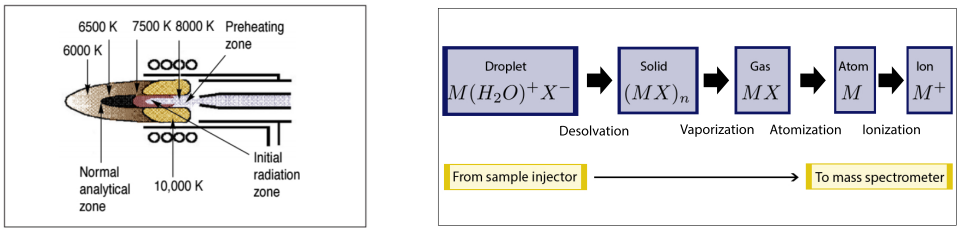

(a) (b)

Figure 2.4: a) Schematic of the different heating zones of the plasma. b) Process of plasma recombination (ionisation).

2.1.3 Interface region

Perhaps the most challenging process of the technique, the interface region allows the ions generated in the plasma to be transferred from atmospheric pressure to the vacuum region and introduced to the mass spectrometer as

an ion beam, serving as a bridge between the ICP and the MS systems [Thomas, 2004]. This region is water cooled, because of the intense heat of the plasma, and comprises the sample cone, the skimmer cone, and the extraction lens[3].

The cones (Figure 2.5) are metallic and conventionally made of Nickel (although, if one wants to avoid corrosion from liquids, platinum cones are more suitable) [Landon, 2006].

In the region after the sampler cone the ion beam expands dramatically due to a pressure reduction. After, only a representative, analyte-rich, fraction of that gas passes on through the skimmer cone and into a region maintained at vacuum.

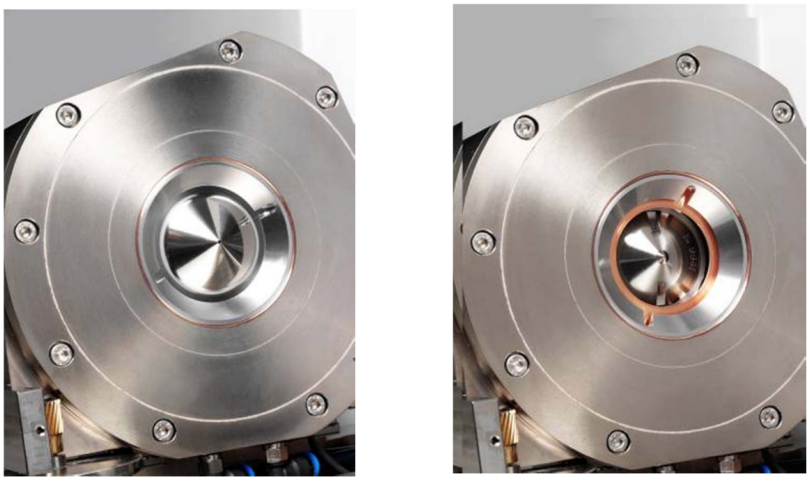

(a) (b)

Figure 2.5: Pictures of the sample (a)) and skimmer (b)) cones. Reproduce from [ThermoScientific, 2013]

[3]A recent innovation has introduced a third cone, the hyper-skimmer, into the interface. Inserted at the exit of the interface region, its purpose is to reduce the divergence of the ion beam, eliminating the need for conventional ion lenses, resulting in an overall improvement of the technique.

2.1.4 Ion-focusing system

The ion-focusing system is an integrant part of the ICP-MS, as it allows for separation of the wanted positive ions from the unwanted neutral species, negative ions and electrons. If this filtering is not done, the system will not work correctly and the signal will be unstable and display background noise. The transfer of the ions from the plasma, which is at atmospheric pressure, through the interface cones and into the mass analyser, which is under high vacuum, is the task of the ion optic system. After passing through the skimmer cone, the ion beam becomes positively charged and, because of the repulsion between all the positively charged ions, separates: in the centre of the beam remain the ions with higher mass-to-charge ratio (m/z ratio) while the ions with lower m/z ratio occupy the outer edges [Thomas, 2004]. This separation due to the m/z ratio is related to the kinetic energy of the ions, the higher the kinetic energy, the higher the transmittance. This is known as the space-charge effect [Thomas, 2001-2002].

Overall, the ion-focusing system is responsible for transferring the maximum possible amount of ions to the mass separation device while rejecting the undesired particles.

2.1.5 Mass analysers

The separation of ions inside the ICP-MS is done based on their mass-to-charge ratio in the analyser region. This separation is done in order to keep the desired ions and remove the unwanted ones. For this effect, different kinds of mass spectrometers exist, each with its own process. Some are, for example, the quadrupole mass filter, the double-focusing sector field and the time-of-flight mass spectrometer [Landon, 2006]. Each of these instruments has pros and cons, mostly regarding speed and cost, and also the mass resolution available [Thomas, 2004]. To this effect, the instrument used should be appropriate to the job in question. Inside the ICP-MS, the mass analyser is placed after the ion-focusing device and before the detector itself, all this at a vacuum of 10^{-6} mbar [Thomas, 2004].

From all the different mass analysers, the quadrupole mass analyser is the most commonly utilised in mass spectrometry. It consists of four parallel cylindrical rods (Figure 2.6) that act as electrodes and to which RF and DC voltages are applied, each voltage to opposite pairs of rods. Depending on the RF and DC voltages applied to the rods, different mass-to-charge ratio ions can be separated. Each specific ion will either show a stable trajectory towards the detector, or show an unstable trajectory that ends in collision with one of the rods of the quadrupole, being neutralised [Cartwright, 2005]. After being transmitted through the quadrupole, ions are guided to the Secondary Electron Multiplier (SEM) and then detected [ThermoScientific, 2013]. With this in mind, we can see that the quadrupole is an adjustable mass filter. On top of this, it also has high scan speeds, providing spectra in less than 100 ms [Thomas, 2001-2002].

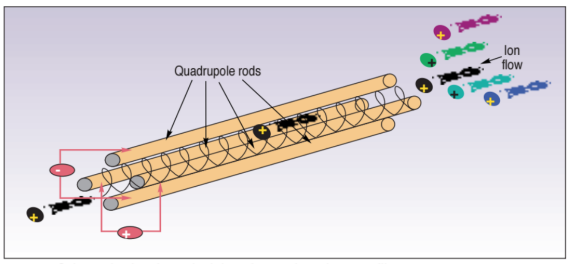

Figure 2.6: Schematic showing principles of mass separation using a quadrupole mass filter.

2.1.6 Interferences

While undoubtedly a powerful analytical technique, ICP-MS is still affected by various interferences that can introduce major errors in the results if not consciously analysed and kept under control. Typically, these can be separated into spectral and non-spectral interferences [Dams et al., 1995]. The first deal with elements presenting the same m/z ratio as the analyte of interest. The second, also known as matrix effects, have to do with influences of the sample matrix on the system. An interference can either enhance or depress the intensity of the analyte.

Spectral interferences

When using ICP-MS, especially a quadrupole based instrument, a common problem encountered is overlapping of certain elemental isotopes by other elements/molecules with similar m/z ratio values.

There are several contributors to this type of interference, the most recognisable are: isobaric, polyatomic and doubly charged species [Dams et al., 1995].

When isotopes from two different elements have the same nominal mass it is called isobaric interference. This can be to some extent circumvented if additional isotopes are monitored and the signal can then be mathematically corrected. A typical example would be quantification of Cd using the most abundant isotope, ^{114}Cd. At this mass channel there would be a contribution from ^{114}Sn, a minor isotope of Sn (abundance 0.65%) that would nevertheless be significant if the sample contains this element. Fortunately, Sn has other isotopes that do not suffer from interferences, such as ^{118}Sn (abundance 24.23%). Thus, one can measure the intensity at ^{118}Sn and use it to calculate the expected contribution for the ^{114}Sn, based on the natural abundance of both isotopes, and correct the data measured at ^{114}Cd from the ^{114}Sn interference, using the following correction equation:

$$I(^{114}\mathrm{Cd}) = I(m/z = 114) - \frac{0.65}{24.23} I(^{118}\mathrm{Sn}).$$

For more complex situations, with multiple interferences, or when the isotopic composition of the samples is different from the natural one, the use of equation corrections is not reliable. Therefore this approach is not always possible and so such interferences remain a large problem [Thomas, 2004].

The second type of spectral interference is the polyatomic or molecular ion interference. It happens when there is a combination of elements, either from the solvent, the sample matrix or the atmospheric gases. This kind of interference is more common when the m/z ratio is below 82, as they contain combinations of atmospheric gases or Ar [Landon, 2006]. A great review of frequently reported polyatomic interferences can be found in [May and Wiedmeyer, 1998].

The last type is the doubly charged ion (M^{2+}). This kind of interference occurs in elements with a low second ionisation potential. Due to the fact that the separation of ions is based on the m/z ratio, doubly charged species show at half the isotopic mass [Thomas, 2004]. Some examples are Sr, Ba (with Zn) and the rare earth elements.

Non-Spectral interferences

Non-spectral interferences occur due to problems with the matrix constituents. These can take many forms, such as scattering effects of ions with matrix atoms, changes in the plasma conditions which lead to a change in the equilibrium between ions and atoms, different viscosities of either samples or standards, deposits of impurities in the cones and memory effects [BiomonotoringMethods, 2012]. The harshest effects occur when the matrix elements are heavier than the element of interest, but other elements have impact.

The plasma temperature, which regulates the state transitions of the analyte is affected by the sample matrix. There is a need to accurately do matrix matching of calibration standards when samples contain large levels of matrix elements [BiomonotoringMethods, 2012]. When the ions are sampled through the cones and focused, interference can also be observed [Landon, 2006]. Due to the fact that the ions are forced to be closer together, repulsion effects occur, mostly in the region behind the skimmer cone. And the lighter ions are the ones that have more ease to move away from the ion beam [Thomas, 2004].

The most common effect of the interferences is the suppression of the signal, caused by increased load on the plasma and also by a lowered efficiency in the ionisation of the element of interest. In some select cases, the contrary can occur, and the interferences lead to an amplification of the signal [BiomonotoringMethods, 2012].

There are ways to minimise these interferences: correction equations, cool plasma technology or matrix separation have been used for several

years [Thomas, 2004]. But the recent introduction of Collision/Reaction Cell (CRC) has proven to be the most reliable method so far, stopping the formation of spectral interferences before they enter the mass analyser.

2.1.7 Collision Cell

The formation of polyatomic spectral interferences can seriously compromise the detection capability of the quadrupole mass analyser. As previously stated these interferences are generated by a combination of Argon, solvent, and/or sample-based ionic species [Thomas, 2004].
CRCs were developed in the late 1990s [Koppenaal et al., 2004] and have been adapted to ICP-MS to stop the formation of many spectral interferences by moving either the interferent or the analyte of interest to another m/z ratio.

CRCs are composed of either a quadrupole, hexapole or octapole cell, located in the interface region of the ICP-MS [McCurdy et al., 2006]. In order to separate the interferent from the analyte, a certain reactive gas, such as hydrogen or helium is introduced into the cell at low pressure. The nature of this gas depends on the system in question, and which interferents are present [McCurdy et al., 2006]. The CRC is operated in RF-only mode that focus all the ions instead of separating them according to m/z ratio, this allows the ions to collide and react with the gas. The reaction of the gas with the ions is what makes it possible to separate them, by converting interfering species into non interfering ones, or it can also convert the analyte into a different ion that is no longer subject to the interference of the initial ions [Thomas, 2004].

For this work a He collision mode was employed. Rather than taking into account the relative reactivity of the species with the reaction gas, this collision cell (Figure 2.7) uses the inert gas to remove all polyatomic species based on their size. Since polyatomics have larger cross-sections then their analog analytes, they collide more frequently with the cell gas and therefore lose more energy as they progress through the cell. The difference in energy at the cell exit allows for separation of the ions: by applying a stopping

voltage one can ensure that only the analytes pass through to the analyser [Thomas, 2004]. This simple and reliable separation process is known as Kinetic Energy Discrimination (KED).

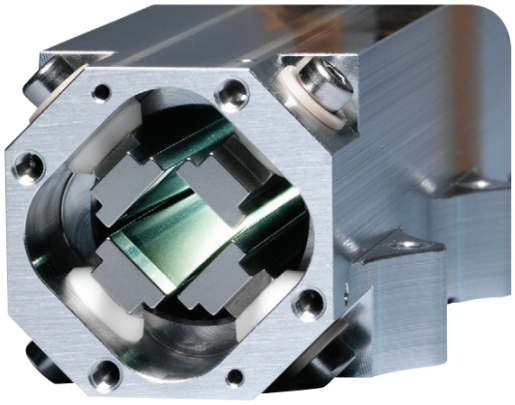

Figure 2.7: Picture of the collision cell (Qcell) entrance.

The use of Helium gives this approach several advantages over the reactive cell gas [Agilent, 2010]. The inert gas does no react with the sample matrix, therefore no new interferences are formed and there's no signal loss for analyte or internal standard ions. The same setup can be used for every sample and there is no need for prior knowledge of the sample matrix, therefore accurate multi-element analysis of unknown and variable sample matrices can be achieved. A more descriptive comparison between the modes can be found in [McCurdy et al., 2006].

2.2 ICP-MS Contamination

Contamination is a problem that all laboratories have to deal with. It is present in any analysis and a hard task to the analist is keeping it to a minimum. This problem is magnified when dealing with trace (< 100 μg/g) and ultratrace (< 1 μg/g) element analysis, which is the case of the extremely high sensitive ICP-MS. Any contamination can lead to a large contribution to the measured concentration and it can reflect in inaccurate data. In order to trust the data there must be great awareness of potential sources of

contamination.

The sample has to go through a series of steps before it is analysed. It is usually collected, stored, processed, and prepared[4] [Richter, 2003]. During all that time the sample comes in contact with many sources of trace metal contamination: laboratory materials, the analyst and airborne contaminants.

When considering the laboratory materials, one should keep in mind that anything that interacts with the sample or its vicinity is a possible source of contamination. One of the most commonly found metals in laboratory materials is Zinc [Richter, 2003]. It is present in glass equipment (e.g. containers or volumetric ware), in paper towels and powdered gloves. Furthermore, all of these can contribute with trace amounts of several other metals (e.g. Fe, Co, Cu). Even coloured pipette tips can contribute with trace amounts of Cu, Fe, Zn and Cd. Avoidance of these materials should therefore be considered and plastic containers should always be used, especially for acidic solutions. Another aspect to take into consideration in order to diminish trace metal contamination from laboratory material is previous washing of all material used to prepare the sample with a dilute acid (1-2% HNO_3 is common).

The sample preparation area and the area around the sample introduction system should be free of airborne contamination. To achieve this a laminar flow hood can be used to keep the air clean and an acrylic enclosure is optimal to keep dust particulates from falling in the samples during the analysis [Richter, 2003].

Adding to the laboratory equipment precautions is the concern of the analyst to not introduce contamination coming from sweat, make-up or even the clothes or jewellery they are wearing. Table 2.1 shows some common trace elements found on the human body.

Perhaps the single most important method for dealing with contamina-

[4]ICP-MS was developed for liquid sample analysis like the ones used in this work. Although it should be noted that when dealing with solid samples an important and complex digestion process has to be implemented before the analysis. For more information refer to [Landon, 2006].

Source of contamination	Trace metal contaminant
Hair	Zn, Cu, Fe, Pb, Mn
Skin	Zn, Cu
Jewellery	Au, Ag, Cu, Fe, Ni, Cr
Cigarette smoke	Cd, As, K, Fe, B
Cosmetics	Zn, Bi

Table 2.1: Common trace elements contaminants found on and around the human body. Adapted from [Thomas, 2004].

tion is the use of an analytical blank throughout the analysis [Richter, 2003]. This allows for quantification of contamination from the sources mentioned above because it has been through all the same steps as the samples.

Besides the above mentioned, there's still the problem of contamination from the instrument itself: peristaltic pump speed, washout times and other ICP-MS parameters should be optimised based on the sample matrix and suite of elements to avoid memory effects in the sample introduction/interface areas and therefore the possibility of contamination from the previous sample being analysed. Also a periodic maintenance of the instrument has to be performed in order to detect signs of corrosion or damage [ThermoScientific, 2013] [Richter, 2003].

ICP-MS is undoubtedly a powerful analytical technique for measuring elements of clinical interest at very low concentrations. It stands out when compared to other present day techniques (a table of comparison is provided in chapter 5). Still its performance is subjected to several possible problems which may affect the reliability of the results. Such factors are usually associated with isobaric and elemental interferences, variations in plasma efficiency, clogging or corrosion of cone apertures and matrix suppression. Also, as previously stated, contamination during recovery and preparation of samples and standards is always a high risk. A combination of processes

can be employed to approach the removal of these detrimental effects and improve the analysis. Some of these processes were mentioned throughout this chapter, and more information on the subject can be found elsewhere.

Like most techniques, ICP-MS is in a constant process of refinement and we should expect much more with future developments.

Chapter 3

Radionuclides in Medical Diagnosis

Radionuclides, or radioisotopes, are chemical elements that have an unstable combination of nucleons, and spontaneously emit radiation in the process of regaining stability. This movement towards stability is known as radioactive decay and it determines the type of radiation emitted: alpha or beta particles, or gamma rays.

The fact that this radiation can be measured and tracked, made it possible for a tremendous variety of man-made radionuclides to find applications in industry, agriculture and, mostly, in Nuclear Medicine, that exploits radionuclides for diagnostic and therapeutic purposes.

3.1 Production of Radionuclides

Although radionuclides can naturally occur (e.g., ^{87}Rb, ^{115}In or ^{137}Cs), all radionuclides used in Nuclear Medicine are produced by one of various routes: neutron activation, nuclear fission, charged particles induced reactions and radionuclide generators [WHO, 2008].

Those produced in nuclear reactors are generally neutron excess nuclides, mostly decay by β^- emission ($^A_Z\mathrm{X} \rightarrow {}^A_{Z+1}X' + e^- + \overline{\nu}_e$) and are suitable for therapy purposes. In comparison, the radionuclides produced in a cyclotron

are generally neutron deficient, and as such decay by β^+ emission (${}^{A}_{Z}\mathrm{X} \rightarrow {}^{A}_{Z-1}\mathrm{X'} + e^+ + \nu_e$) or electron capture (${}^{A}_{Z}\mathrm{X} + e^- \rightarrow {}^{A}_{Z-1}\mathrm{X'} + \nu_e$). Due to these characteristics, they are more suited to use in diagnosis, and the β^+ are often used in Positron Emission Tomography (PET) [Ahmad, 2013].

The following sections present some of the most important aspects of cyclotrons and generators.

3.1.1 Cyclotron

In a cyclotron charged particles are accelerated to high energies. The cyclotron uses a magnetic field to bend the moving particles into a circular path, so that they can be repeatedly accelerated by the same electric field. The resulting beam, with the desired energy, is directed towards a suitable target, inducing a nuclear reaction.

The initial design of the cyclotron was made with nuclear physics research in mind. It was created in 1930 by E. O. Lawrence and over the years it has changed to accommodate the increasing demand in both particle energy and beam intensity needed for scientific research. Despite the initial purpose, the practical applications of the cyclotron in medicine were already predicted by Lawrence at that time, as well as the use of the newly discovered radioisotopes both in chemical and biological studies. Today, imaging diagnosis and different disease treatments deeply rely on accelerator produced radioisotopes.

Through the years many improvements were made to the device but its principle still remains the same. Currently, cyclotrons are the most used type of particle accelerator for the production of PET radiopharmaceuticals.

Principles of Operation

A cyclotron accommodates in a vacuum chamber two or more hollow copper electrodes, also known as *dees*, in reference to their original shape (Figure 3.1(a) and 3.1(b)).

A high radio-frequency power supply is connected to both *dees* providing

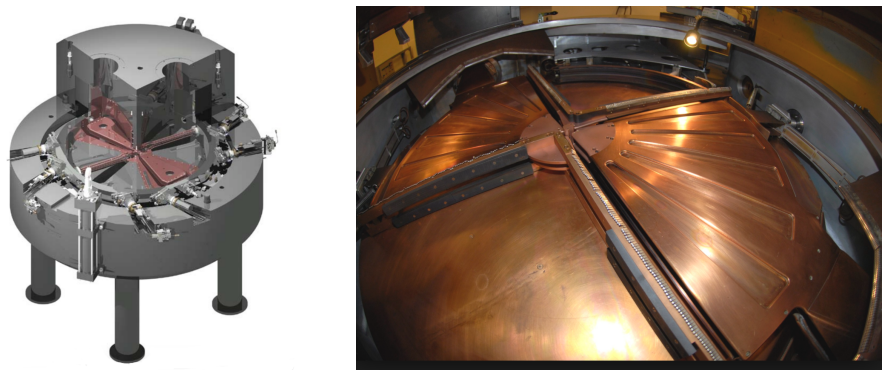

(a) (b)

Figure 3.1: a) Illustrative image of a cyclotron (Cyclone 18/9) from IBA Molecular. b) Picture of the interior of a cyclotron showing two hollow copper electrodes or *dees*.

a sinusoidal alternating electric field between them, while maintaining the field close to zero inside them, as represented in the basic schematic view of a cyclotron in Figure 3.2. This electric field will accelerate ions such as H^- or D^-. Along with the electric field, the ions are subjected to a magnetic field perpendicular to their trajectory, as the whole vacuum chamber is placed between the poles of a large magnet. The charged particle under these conditions experiences the effect of the Lorentz force (equation 3.1),

$$\overrightarrow{F} = q[\overrightarrow{E} + (\overrightarrow{v} \times \overrightarrow{B})], \tag{3.1}$$

which provides the necessary centripetal force responsible for turning the straight trajectory of the particles into a spiral trajectory inside the *dees*. Here, q and $\overrightarrow{v}$ are the charge and velocity of the particle, respectively, $\overrightarrow{E}$ is the electric field, $\overrightarrow{B}$ the magnetic field and $\overrightarrow{F}$ the Lorentz force.

The Lorentz force is directed perpendicular to both the direction of the magnetic field and the direction of the particle orbit, and points approximately towards the centre of the cyclotron. The magnitude of the force is proportional to the magnitude of the magnetic field and to the velocity of the particle.

The ion source, a small chimney (Figure 3.3) placed between two negative

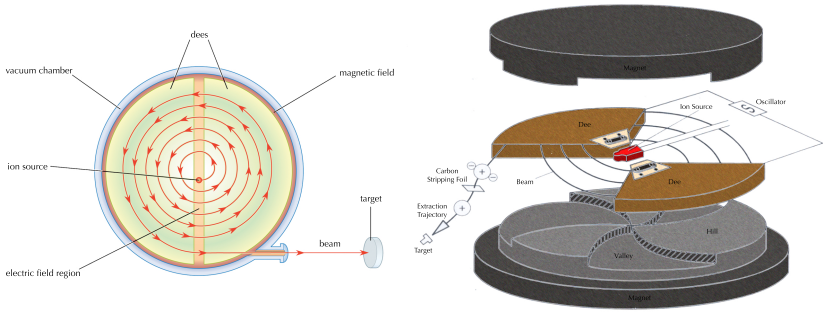

Figure 3.2: Schematic diagram of a cyclotron depicting the position of the on source and the magnets. A simplified view of the particle's trajectory is also sketched.

high-voltage cathodes, is located in the centre of the cyclotron. To produce negative ions, a gas, either Hydrogen or Deuterium, is introduced in that chimney and a high voltage is applied. The negative ions are extracted from the ion source and accelerated into one of the *dees*, starting their spiral trajectory through the cyclotron.

Figure 3.3: Example of chimneys, cathodes and puller. Two copper - tungsten chimneys at the back (note that the chimney on the right shows an eroded slit). Two tantalum cathodes up front (they are shaped to reduce heat conduction and the material allows for high electron emission). In the middle is a *puller* or extraction electrode, it is used to extract the beam from the ion source to the accelerating region inside the cyclotron. Its alignment with the chimney aperture is critical to the initial launch angle. Image adapted from [Kleeven and Zaremba, 2015].

It should be made clear that inside the *dees* the particles are only subjected to the magnetic field, it is only in the gap between the two that the electric field acts and accelerates them.

If the current *dee* is positively charged, the *counter-dee* is negatively

charged, accelerating the ion when it passes from one to the other. Afterwards the polarity is reversed and the process repeats, but now, the ion has a slightly larger orbit inside the *dee*, as a result of its increased speed.

The acceleration process happens repeatedly until the ion's trajectory fills the entire cyclotron. When the ions reach the outer radius of the chamber, they are stripped of their electrons, thus becoming positively charged. Extraction of the beam from the system is then achieved as a result of the now opposing Lorentz force. There is more than one way of extracting the beam [Kleeven, 2004]. One well-known method for negatively charged particles is, as stated, the extraction obtained by passing the beam through a thin carbon foil (stripper), hereby stripping the negative ions of their electrons and turning them into positive ions. The cyclotron used in this project has this type of extraction system, holding multiple extraction ports around it. A schematic can be seen in Figure 3.4. This technique is simple in comparison to others and allows for an extraction efficiency close to 100% [Kleeven, 2004].

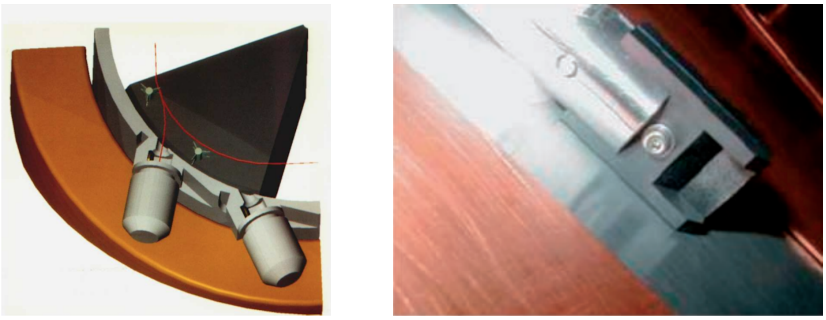

(a) (b)

Figure 3.4: a) Schematic of multiple extraction ports in a cyclotron. b) Image of a thin carbon stripper foil.

After extraction, the ion travels towards the target position, colliding with a specific substance, either liquid or gas. If this positively charged bombarding particle has sufficient kinetic energy to overcome the Coulomb barrier and the negative Q value, there is the possibility of a nuclear reaction taking place. And so, conserving the nucleons, charge, energy and momentum, it is possible to produce the desired radioisotopes.

The energy of the incident particles before the intersection with the target is related to the radius the ions trace inside the *dees*. The greater the acceleration of the ions, the larger the radius they trace. The energy of the projectiles is expressed by equation 3.2,

$$E_{kin} = \frac{1}{2}\frac{q^2}{m}B^2r^2 \tag{3.2}$$

where q is the charge and m is the mass of the ion, B is the modulus of the magnetic field vector and r is the radius of the trajectory of the ion inside the *dees*. The energies that can be achieved in the cyclotron depend on the ion, the radius of the cyclotron and on the size of the magnet.

3.1.2 Generators

Generators are a convenient source of short-lived radionuclides, proven to deliver high specific activity and easily made available at sites remote from cyclotron facilities [Vértes et al., 2011].

Historically known as "cows", generators effectively separate radioactive daughter nuclides from their decaying, long-lived, parent nuclides based on the decay-growth relationship between the two [Vértes et al., 2011]. Sufficient chemical difference between the species is essential in order to optimise the separation method [Saha, 2010].

The generator operation is fairly straightforward consisting of a column in which the long-lived radionuclide (parent) is bound to a solid adsorbent chemical matrix[1], such as Al_2O_3, TiO_2 and ZrO_2. The daughter radionuclide grows as a result of the decay of the parent until either a transient or a secular equilibrium is reached within several half-lives of the daughter. This condi-

[1]This is by far the predominant separation method in the field of radionuclide generators. Other emerging techniques include: solvent extraction, thermo separation, precipitation and electrochemical separation. Further information can be found in [Dash and Chakravarty, 2014]

tion is the principle underlying generator production of short-lived isotopes for use in nuclear medicine, such as ^{99m}Tc, ^{113m}In and lately ^{68}Ga.

Transient equilibrium occurs when the half-life of the parent radionuclide is longer than the half-life of the daughter radionuclide by a factor of 10 or more. After the time required to achieve transient equilibrium has elapsed, the daughter will be formed at a rate determined by the half-life of the parent, but will also be decaying at a rate set by its own half-life [Phillips, 1996]. The number of daughter atoms, N_2, present at any later time is given by equation 3.3,

$$N_2 = N_2^0 e^{-\lambda_2 t} + \frac{\lambda_1}{\lambda_2 - \lambda_1} N_0 (e^{-\lambda_1 t} - e^{-\lambda_2 t}), \tag{3.3}$$

where N_0 is the number of parent atoms and N_2^0 is the number of daughter atoms at $t = 0$, λ_1 is the decay constant of the parent radionuclide and λ_2 is the decay constant of daughter radionuclide [Dash and Chakravarty, 2014]. The decay constant is inversely proportional to the half-life of the radionuclide, $\lambda = 0,693/t_{1/2}$. Transient equilibrium for the transition ^{99}Mo ($t_{1/2} = 66h$) $\rightarrow$ ^{99m}Tc ($t_{1/2} = 6h$) is illustrated in Figure 3.5(a) and 3.5(b).

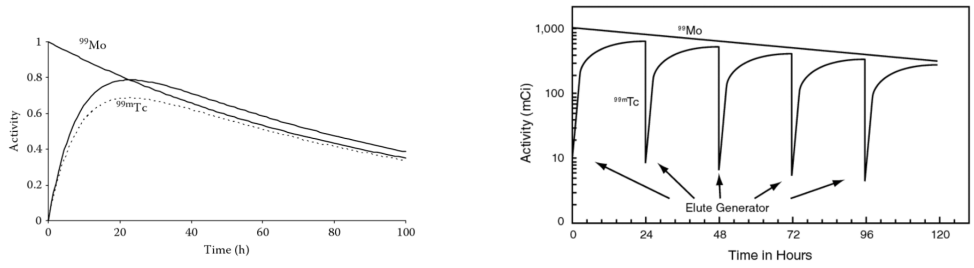

(a) (b)

Figure 3.5: a) Plot of ^{99}Mo and ^{99m}Tc activity versus time for an elution in a ^{99}Mo/^{99m}Tc generator. The graph depicts the direct application of equation 3.3 for ^{99m}Tc (solid curve), and the curve expected if taken in consideration the fact that only 87% of the decays result in 140keV gamma rays (dashed curve). Adapted from [Abrunhosa and Prata, 2008]. b) Plot of typical ^{99}Mo and ^{99m}Tc activity (logarithmic scale) versus time for multiple elution of a ^{99}Mo/^{99m}Tc generator.

Secular equilibrium may occur when the half-life of the parent radionuclide is many times greater than the half-life of the daughter radionuclide,

by a factor of 10^4 or more. In this case, $\lambda_1 \ll \lambda_2$, and equation 3.3 may be simplified by assuming $\lambda_2 - \lambda_1 \approx \lambda_2$ and that $e^{-\lambda_1 t} = 1$,

$$N_2 \approx \frac{\lambda_1}{\lambda_2} N_0 (1 - e^{-\lambda_2 t}), \tag{3.4}$$

assuming the condition right after elution, meaning the initial activity of the daughter radionuclide is zero, $N_2^0 = 0$. Secular equilibrium is reached after several half-lives of the daughter have elapsed, $e^{-\lambda_2 t} \approx 0$, and the activities of parent and daughter nuclides are equal, $\lambda_2 N_2 = \lambda_1 N_1$ (Figure 3.6).

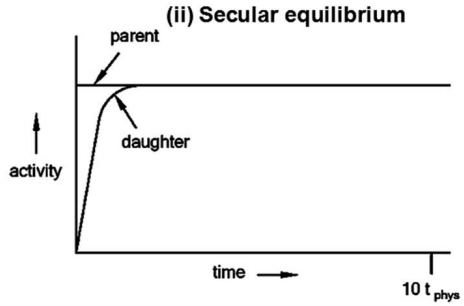

Figure 3.6: Example of secular equilibrium activity versus time. Adapted from [Dash and Chakravarty, 2014].

After an equilibrium condition is reached, the column is flushed with a suitable solution (e.g., hydrochloric acid) that elutes the daughter and leaves the remaining parent on the column. After elution, the daughter activity starts to grow again [Bronzino and Peterson, 2015].

Following its development in 1957 by Powell Richards, the ^{99}Mo/^{99m}Tc generator system has been used to routinely produce the radionuclide ^{99m}Tc. It is estimated that about 80% of all diagnostic nuclear medicine procedures use radiopharmaceuticals labeled with ^{99m}Tc [IAEA, 2010].

3.2 Positron Emission Tomography

Positron emission tomography, PET, is a method for medical research and clinical routine diagnostics. Its purpose is to study normal and abnormal organ physiology by, non-invasively and in vivo, detecting biochemical changes

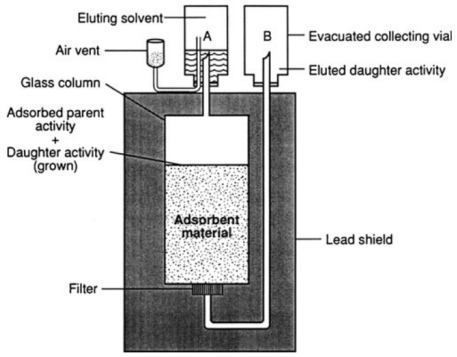

Figure 3.7: a) Schematic of a typical generator system based on column chromatographic separation. The eluent in vial A is passed through the column and the daughter nuclide is collected in vial B under vacuum.

that could be affecting the organ's functional integrity.

The concept of positron emission tomography was introduced in the 1950s by David E. Kuhl, Luke Chapman and Roy Edwards, but the first PET camera was only completed in January 1974 by Michael Phelps, Edward Hoffman and Michael M. Ter-Pogossian [Steiner, 2002]. With the advances in technology and materials, by the 1990s, PET experienced an accelerated development and became more than a research tool, being finally recognised as clinically relevant. Since then it has become the imaging method of choice in the field of Nuclear Medicine, largely owing that status to the availability and success of the radiotracer fluorodeoxyglucose (2-deoxy-2-[^{18}F]-fluoro-D-glucose (FDG)). FDG was first synthesised in 1976 in Brookhaven for PET scanning. Louis Sokoloff and Martin Reivich came up with the idea of radioactively tagging 2-deoxyglucose as a way to image metabolic activity in the brain [Brookhaven National Laboratory, 2012]. They turned to Joanna Fowler and her Brookhaven chemistry group (who had at the time pioneered the development of ^{18}F-labeled elemental fluorine gas) to make this possible [Fowler and Ido, 2002]. Today, FDG is the world's most widely used radiotracer for cancer diagnosis.

The need for imaging agents with disease specification action continues to drive PET growth. In this field ^{68}Ga has a significant contribution to make.

In this section a few aspects of PET will be reviewed, it's not intended to

be an exhaustive analysis but it should be enough to mark the importance of this technique and the motivation for this work.

3.2.1 Basic concepts and application

This non-invasively method relies on short-lived positron-emitting radioisotopes which, combined with metabolic chemical molecules (carrier molecules), form the radioactive tracer. These tracers are injected into the human body for clinical examinations and medical research. Since each carrier is specific to one kind of family of molecules the tracer will accumulate in certain sites in the body depending on its biochemical structure.

Images from a PET scan display bright spots where the radioactive tracer collected, exposing different levels of activity and therefore information about the organ or tissue.

When comparing the different imaging techniques in use nowadays, PET clearly has the upper hand. Although other techniques, like Single Photon Emission Computed Tomography (SPECT), are considerably cheaper, PET offers an increased sensitivity as a result of electronically performed collimation. This in turn allows for a smaller amount of tracer to be injected without loss of image quality [Rahmim and Zaidi, 2008]. Moreover, PET has high specificity and accuracy when measuring *in vivo* molecular interaction [Saha, 2004] and based on metabolic function, distinguish benign from malignant masses [Griffeth, 2005].

There's a vast range of clinical fields where the use of PET imaging can make a difference. Along with the detection and evaluation of the treatment of cancer, PET scans also provide information about other conditions in several organs and/or tissues. Some specific examples of neurological applications include the diagnose of conditions such as epilepsy, Alzheimer's disease, Parkinson's disease, cerebrovascular accident and more. Additionally, PET can be used to detect hematoma or perfusion of the brain tissue and to locate a specific surgical site prior to the procedure.

For some time now, the combination of PET with Computed Tomography (CT) scans, providing co-registration of the two images (PET/CT), is the common way to perform PET procedures. This allows for more accurate diagnoses because it generates images that combine both great anatomic detail and physiologic information [Griffeth, 2005].

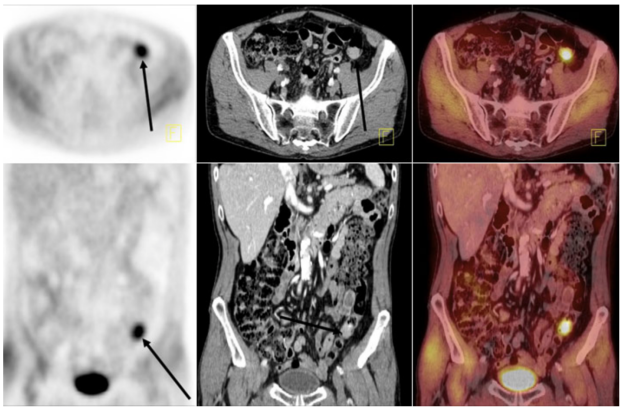

Figure 3.8: Axial and coronal images from PET/CT scan. PET images are on the left, CT images in the center, and PET/CT fusion images on the right.

3.2.2 Common PET radionuclides

The most suitable positron-emitting isotopes for labelling are those that do not disturbe the biological function of the different biomolecules. Among the many existing isotopes ^{11}C, ^{13}N, ^{15}O and ^{18}F are the most commonly used for imaging biological systems. Some of their most relevant characteristics are presented in Table 3.1, alongside other radionuclides of increasing importance.

The shorter half-lives of ^{11}C, ^{13}N, and ^{15}O make them ideal to study processes that have rapid uptake. On the other hand, ^{18}F, with an approximately two-hour half-life, allows more time for synthesis and for imaging somewhat longer physiologic processes as well as for distribution to sites without a cyclotron. The radionuclide ^{64}Cu with its low-energy positrons and longer half-life is a suitable for slow metabolic studies.

Additional information on the radionuclides above, as well as decay properties and production mode of some long-lived positron emitters can be found

Radionuclide	Half-life	$E_{max}(keV)$	Radiation	Production method
Positron emitters				
^{11}C	20.4 min	961	$\beta^+(\%100)$	$^{14}\mathrm{N}(p,\alpha)^{11}\mathrm{C}$
^{13}N	9.97 min	1190	$\beta^+(\%100)$	$^{16}\mathrm{O}(p,\alpha)^{13}\mathrm{N}$
^{15}O	2.05 min	1700	$\beta^+(\%100)$	$^{14}\mathrm{N}(d,n)^{15}\mathrm{O}$
^{18}F	109.8 min	634	$\beta^+(\%97)$	$^{18}\mathrm{O}(p,n)^{18}\mathrm{F}$
^{64}Cu	12.8 h	656	$\beta^+(\%19)$	$^{64}\mathrm{Ni}(p,n)^{64}\mathrm{Cu}$
^{66}Ga	9.5 h	4153	$\beta^+(\%56)$	$^{66}\mathrm{Zn}(p,n)^{66}\mathrm{Ga}$
^{68}Ga	67.6 min	1899	$\beta^+(\%89)$	$^{68}\mathrm{Ge}/^{68}\mathrm{Ga}$ Generator $^{68}\mathrm{Zn}(p,n)^{68}\mathrm{Ga}$
^{124}I	4.17 d	2100	$\beta^+(\%23)$	$^{124}\mathrm{Te}(p,n)^{124}\mathrm{I}$

Table 3.1: Selected radionuclides used in clinical PET, their production mode and decay properties.

in [Saha, 2010] and [Vértes et al., 2011].

3.2.3 Detection Principle

As previously mentioned, PET uses sensors to detect the unique decay characteristics of radionuclides decaying by positron emission. These radionuclides are generally chosen for their capacity to bond to organic molecules and, as such, act as tracers for certain physiological activities inside the body.

As the neutron-deficient radionuclides decay towards stability inside the body, a transformation of a proton into a neutron - with the emission of a neutrino and a positron - occurs. The use of PET relies on the ability to detect the results of the positron annihilation process ($p \rightarrow n + e^+ + \nu_e$).

Shortly after being produced, the positrons interact with free electrons in the medium and annihilate into two photons ($e^+ + e \rightarrow \gamma + \gamma$), as can be seen in Figure 3.9.

In acordance with the energy E to mass m equivalence $E = mc^2$, both these photons have an energy of 511 keV and are emitted 180° from each other. It is this property of the rays being emitted in opposite directions and

their capacity to escape the body that allows to locate the origin.

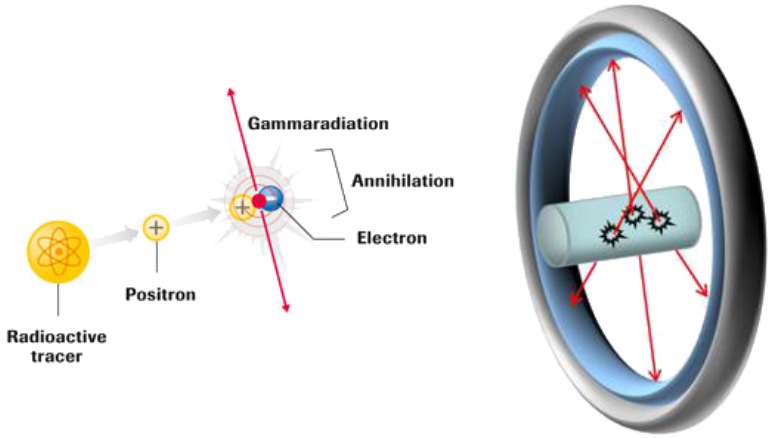

Figure 3.9: Principle of PET detection. Tracers emitting positrons are used as imaging agents for PET. The positron travels a short distance before it annihilates with an electron to give two photons of 511 keV travelling under a mutual angle of 180°. The simultaneous detection of these two gamma ray photons is behind the PET principle and allows in vivo quantitative 3D imaging acquisition. Adapted from Gallery of Wilhelm Imaging Research and [Velikyan, 2014]

The detection of this event is made by matching simultaneous signals in the detectors surrounding the source. When two photons are simultaneously recorded by a pair of detectors, the annihilation event that originated them must have occurred somewhere along the line connecting the detectors, called a Line of Response (LOR). By continuously scanning the body, it is possible to reproduce a 3D image of the distribution of the tracer inside the organism [Caramelo et al., 2008].

Chapter 4

The Radionuclide ^{68}Ga

Finding new and reliable radiopharmaceuticals specific for particular diseases is one of the driving forces behind the expansion of clinical PET. Sometimes going back and reviewing what was set aside is the best way to move forward. That's fairly what happened with the metallic positron emitter ^{68}Ga. With the introduction of the first radionuclide generators in the early 1960s came the development of ^{68}Ga-based imaging agents [Velikyan, 2014]. Sadly, the conditions at the time were not fully developed, mostly there was lack of a reliable source, because the generator's design was inadequate for ^{68}Ga radiopharmaceutical synthesis [Velikyan, 2014]. Besides, a rapid development of ^{99}Tc and ^{18}F was taking place and showing great promise, so all efforts were redirected towards them.

However, a *renaissance* of ^{68}Ga radiopharmacy has come about of late, in large part as a result of the development of small tumour-affine peptides targeting somatostatin receptors[1]. There has been a tremendous increase in the number of publications reflecting the success of ^{68}Ga in clinical studies [Khan et al., 2009] [Eberlein and Lassmann, 2013] [Prata, 2012] [Banerjee and Pomper, 2013].

The ^{68}Ge/^{68}Ga generator system is still the most common way to obtain ^{68}Ga. Such systems are simple to use and relatively inexpensive, ideal for a

[1]Somatostatin (STT) is also known as Growth Hormone-Inhibiting Hormone (GHIH) [Baum and Rösch, 2013]. It is a peptide hormone that regulates the endocrine system and affects neurotransmission and cell proliferation.

site located far from a cyclotron facility. Production of ^{68}Ga from medium to low energy cyclotrons has also been researched and, so far, the reaction $^{68}\mathrm{Zn}(p,n)^{68}\mathrm{Ga}$ is one of the most promising, as is presented further ahead.

Many recent articles recognise ^{68}Ga-labeled peptides as a new class of radiopharmaceuticals with faster blood clearance and target identification [Banerjee and Pomper, 2013]. Among the (numerous) currently studied radiopharmaceuticals, the most prominent are ^{68}Ga-DOTA-NOC, ^{68}Ga-DOTA-TOC and ^{68}Ga-DOTA-TATE [Virgolini et al., 2010].

4.1 Basics of chemistry and labelling

Unlike ^{11}C, ^{68}Ga does not have a natural biochemical function, that we know of, [Green and Welch, 1989] but its coordination chemistry is still of great interest and many applications are being discovered in radiopharmacy. A brief summary of the most important aspects of gallium chemistry is presented. Its coordination chemistry has been reviewed in detail elsewhere [Prata, 2012].

Gallium is a metal classified as a hard acid, together with Indium and other Group III elements. Under physiological conditions, the stable state is Ga^{3+}, with a +3 oxidation. Gallium easily forms bonds with ionic and non polarisable Lewis bases like nitrogen and oxygen atoms [Prata, 2012].

The coordination chemistries of gallium (III) and iron (III) are very similar (concerning charge, preference of the coordination number 6 and even similarities in the ionic radius, 62 and 65 pm respectively), and this affects the use and preparation of gallium radiopharmaceuticals. Transferrin, a highly concentrated plasma protein, is responsible for iron transport, having two sites of binding to that element [Velikyan, 2014]. These sites also have high affinities for Ga^{3+}, so if a low stability ^{68}Ga-complex is injected in the body almost all of the metal will be complexed by the protein, which would result in liver and lung accumulation of the metal [Fani et al., 2008].

The hydrated cation Ga (III) in a solution is unstable - hydrolysing when the pH of the solution is high enough. This makes it impossible to prepare gallium radiopharmaceuticals in water with pH close to 7. This hydrolyse leads to the creation of the hydroxide $Ga(OH)_3$, which is insoluble

[Prata, 2012]. This means that the cation Ga (III) is stable only in acidic conditions. The creation of the hydroxide $Ga(OH)_3$ can be avoided if certain stabilising weak ligands are present in the solution. These include acetate, citrate or 4-(2-hydroxyethyl)-1-piperazineethanesulfonic acid (HEPES) [Roesch and Riss, 2010].

If a radiopharmaceutical is to be used practically, it must adhere to certain conditions. The first being that at the pH levels present in the organism, the compound must be thermodynamically stable, and also, the compound must be inert in the time scales of the clinical use [Morgat et al., 2013]. There are two types of labelling that can be done with radiometals such as Ga(III). The first is the direct labelling of macromolecules with ^{68}Ga, but it shows limited applications to proteins, such as lactoferrin, transferrin and ferritin, which are naturally designed for iron binding. The second method is called chelator-mediated labelling, and it is the most commonly used in imaging [Velikyan, 2014]. It starts by first synthesizing a bioconjugate comprising vector molecule and chelate moiety, which coordinates the radiometal ion.

The chelator most used in labelling for +3 oxidation radiometals is a macrocyclic called DOTA [Fani et al., 2008]. In clinical studies, the analogues frequently used are: ^{68}Ga-DOTA-TOC, ^{68}Ga-DOTA-TATE and ^{68}Ga-DOTA-NOC (Figure 4.1). They show compatibility with the half-life of ^{68}Ga in their blood clearance, target localisation rate and pharmacokinetics. The analogues show high sensitivity and resolution, short scanning times and the ability of renal excretion, all this together correlates to high quality, high contrast images with accurate quantitation of the organs in study. Seeing as these are to be used in living organisms, the relatively low radiation dose is also a positive point. They have been used in diagnosis, prognosis, staging, therapy selection and in response monitoring different kinds of diseases and cancers, such as NeuroEndocrine Tumours (NET)s [Velikyan, 2014].

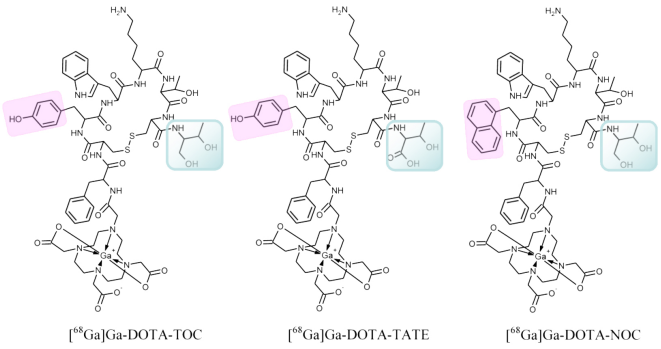

Figure 4.1: Structural formulae of the most clinically used somatostatin analogue imaging agents: TOC, TATE and NOC . The differences in structures are highlighted. From [Velikyan, 2014].

4.2 ^{68}Ge/^{68}Ga Generators

As mentioned in chapter 3.1.2, radionuclide generators contain a relatively long-lived parent nuclide that decays to a shorter-lived daughter nuclide. In this particular case, all the necessary conditions for having a generator pair are present: there's sufficient chemical difference between them and the half-lives, ^{68}Ge-$t_{1/2}$ = 270.8 days and ^{68}Ga-$t_{1/2} \approx$ 68 min, are suitable for radiopharmaceutical synthesis (Figure 4.2(b)) [Prata, 2012].

Figure 4.2(a) shows an example of a lead-shielded, yet portable, and commercially available ^{68}Ge/^{68}Ga generator. Inside the chromatographic separation columns, either an inorganic matrix such as TiO_2 or SnO_2, or an organic polymer is present, in which the ^{68}Ge is kept. Using hydrochloric acid in an appropriate concentration (0.05−1 M), $^{68}Ga^{3+}$ can be easily eluted from the system as a final product[Abrunhosa and Prata, 2008].

In currently available generators, the concentration of ^{68}Ge in the eluate has been the subject of many studies and has been found to be acceptably low, delivering ^{68}Ga in a high chemical purity [Mueller et al., 2016]. Apart from ^{68}Ge, other metal ions (e.g., Fe, Zn, Al and Cu) if present in the eluate can compete with Ga^{3+} for the chelator and have a high impact on the labelling efficiency. Therefore, such impurities in the generator eluate and in

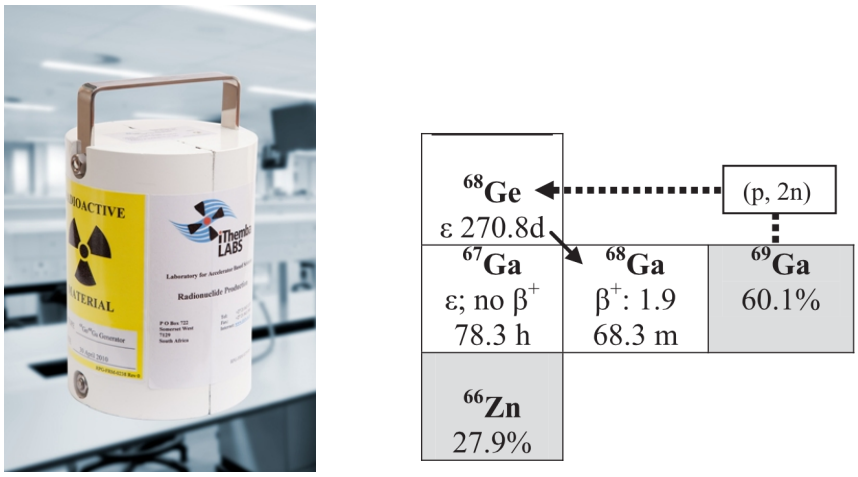

(a) (b)

Figure 4.2: a) Example of a ^{68}Ge/^{68}Ga generator. b) Production of ^{68}Ge by the $(p, 2n)$ reaction of ^{69}Ga. From [Maecke and André, 2007].

the labelling reagents have to be avoided [Šimeček et al., 2012].

4.3 ^{68}Zn$(p,n)^{68}$Ga excitation function

In order to choose the most appropriate energy for a nuclear reaction one has to make a study of the reaction's cross section as a function of the incident charged particle energy. This is usually known as the excitation function. Several methods of production for the accelerator obtained ^{68}Ga have been studied [Aslam et al., 2014] [Tel et al., 2011] [Szelecsényi et al., 1998].

So far, the reaction that seems most suitable, for energies up to 30 MeV, is the ^{68}Zn$(p,n)^{68}$Ga ($E_{thr} = 3.76$MeV). The data Tel *et al* obtained, through simulations using nuclear reaction models, and its comparison to several experimental values for the proton-induced reaction is shown in Figure 4.3. According to such data, we can expect the optimum energy for the production of ^{68}Ga to be in the 5−15 MeV range. Proton with energies in this range will maximise the production yield of ^{68}Ga and minimise radioactive impurities. This is also the reaction used at ICNAS for the production of the ^{68}Ga.

The problem with using this reaction is the production of ^{67}Ga ($t_{1/2} =$

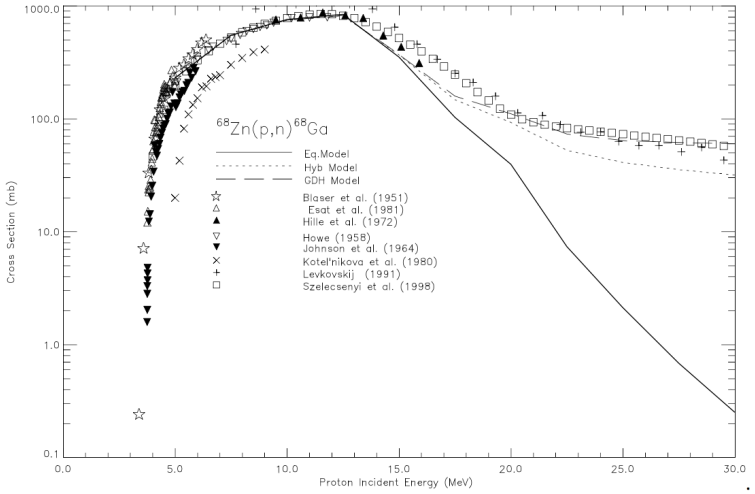

Figure 4.3: Comparison of calculations of the excitation functions with the experimental data for the $^{68}\mathrm{Zn}(p,n)^{68}\mathrm{Ga}$ reaction. The experimental datasets are taken from EXFOR data files. Adapted from [Tel et al., 2011].

78, 3h), a gamma - emitter, by the reaction channel $^{68}\mathrm{Zn}(p,2n)^{67}\mathrm{Ga}$ (Figure 4.4).

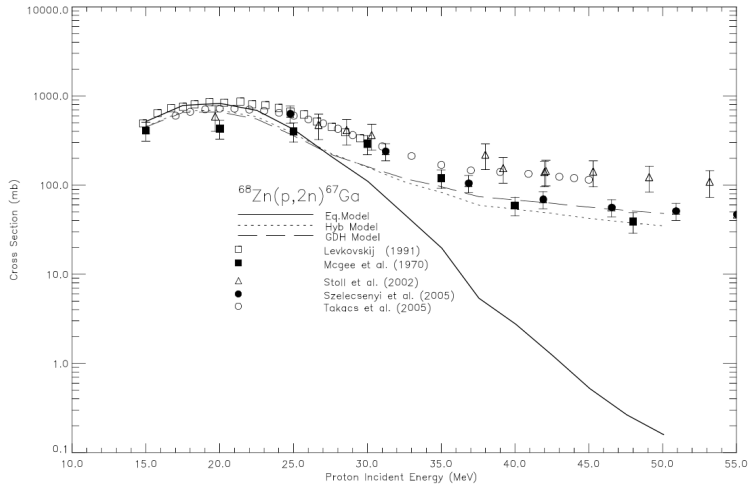

Figure 4.4: Comparison of calculations of the excitation functions with the experimental data for the $^{68}\mathrm{Zn}(p,2n)^{67}\mathrm{Ga}$ reaction. The experimental datasets are taken from EXFOR data files. Adapted from [Tel et al., 2011].

The presence of the long-lived contaminant limits the application period of the ^{68}Ga final product. Radio-gallium contamination-free production of

^{68}Ga requires the use of highly enriched target material and, due to the relatively low starting energy of the $^{68}\mathrm{Zn}(p, 2n)^{67}\mathrm{Ga}$ reaction ($\mathrm{E_{thr}} = 12.16\mathrm{MeV}$), that maximum bombarding energies should be limited to $12,16\mathrm{MeV}$.

4.4 Application to PET imaging

In the field of clinical nuclear medicine, interest in ^{68}Ga mainly arose due to the remarkable success of ^{68}Ga-labelled peptides in PET imaging of NETs [Ambrosini, 2014]. NETs originate in cells of the nervous and endocrine systems and are considered a class of rare tumours. Since the 1990's, SST analogues (STTa) have been used for imaging and evaluation of NETs and, at the time, the radiopharmaceutical ^{111}In-pentetreotide (Octreoscan) presented great results. Octreoscan is a scintigraphic study used in nuclear medicine to find different types of tumours such as carcinoid, pancreatic and neuroendocrine tumours, and to localize sarcoidosis [Hanson, 2001]. In light of recent discoveries and developments, like the conjugation of PET and CT, ^{68}Ga-labelled STTa (mostly ^{68}Ga-DOTA-STTa) were found to have higher affinity for somatostatin receptors and many studies are proposing them as an alternative for Octreoscan [Schubiger et al., 2007].

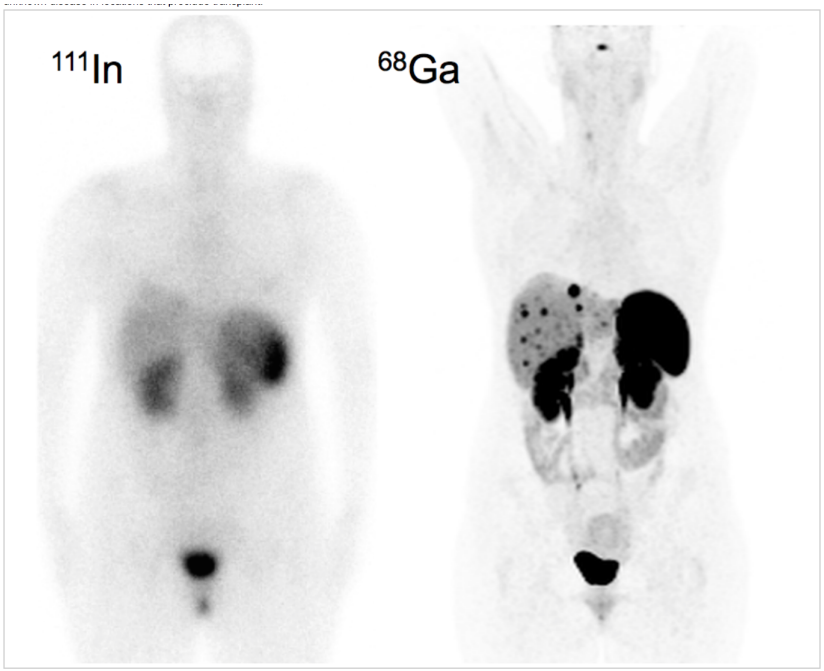

Figure 4.5: Images of a carcinoid tumor patient obtained with both ^{68}Ga-DOTA-NOC and ^{111}In-Octreoscan. In contrast to the ^{111}In image (left), which appears normal, the ^{68}Ga image (right) reveals multiple metastatic lesions in the liver [Mathias et al., 2015].

All in all, ^{68}Ga has been a big promotor of research in the PET-field by being widely used as a label for different compounds, biological macromolecules, and even nano-particles [Velikyan, 2014]. The largest use of ^{68}Ga in PET imaging is still in oncology, but it is not the only one. Application to the imaging of myocardial, pulmonary and cerebral perfusion, inflammations and infections, blood-brain barrier defect, apoptosis, hypoxia, glycosis, angiogenesis and even to image brain and bone have all been investigated [Green and Welch, 1989]. ^{68}Ga is in a way seen as an analogue of ^{99m}Tc for PET diagnosis, but providing a higher resolution and higher sensitivity process, together with advantages of dynamic scanning and personalised medicine [Banerjee and Pomper, 2013] [Roesch and Riss, 2010].

Chapter 5

Methods and Materials

5.1 Instrumentation

A Thermo Scientific iCAP Qc ICP-MS (Figure 5.1) was used to carry out all measurements. In addition, a helium collision cell was employed in all experiments to help remove interferences by the KED method.

Figure 5.1: Front view of the iCAP Qc MS used for this work.

Some important instrument parameters are listed in Table 5.1.

The RF power and the flow rates may vary with each calibration performed on the apparatus. In fact, there is a multitude of interrelated vari-

ICP-MS parameters	
Argon flow	24 L/min
Argon pressure	$5.5 - 6$ bar
Helium flow	10 L/min
Helium pressure	$0.5 - 1$ bar
RF power	1550 W
main runs	3
uptake time	110 s
wash time	60 s

Table 5.1: ICP-MS operating conditions.

ables (e.g. sampling depth, torch design, torch position, ion lens settings) that have to be optimised for each operation in order to obtain the highest signal intensity and the best detection limit [McCurdy et al., 2001].

Finding the adequate technique for a certain application is not easy. Table 5.2 lists some criteria that should be considered when choosing a technique. A comparison is made for Flame AAS, Graphite Furnace AAS, ICP-OES and ICP-MS [PerkinElmer, 2009]. ICP-MS was identified as the most suitable for our needs: multiple elements analysis in the trace and ultra-trace analyte concentrations.

	ICP-MS	ICP-OES	Flame AAS	GF-AAS
Detection limits	Excellent for most elements	Very good for most elements	Very good for some elements	Excellent for some elements
Sample throughput	all elements 2-6 min	5-30 elements/min	15s/ element	4 min/element
Linear dynamic range	10^5(10^8 with range extension)	10^4 to 10^8	10^3	10^2
Isotopes	yes	no	no	no
No. of elements	> 75	> 75	> 68	> 50
Sample usage	low	low	very high	very low
Semi-quant analysis	yes	yes	no	no
Operating cost	high	high	low	medium

Table 5.2: Simplified comparison of some important aspects to take in consideration when selecting an atomic spectroscopy technique. Adapted from [Tyler, 2015].

The usefulness of an analytical technique is greatly determined by the detection limits the technique achieves for individual elements. Typical detection-limit ranges for the major atomic spectroscopy techniques are shown in Figure 5.2.

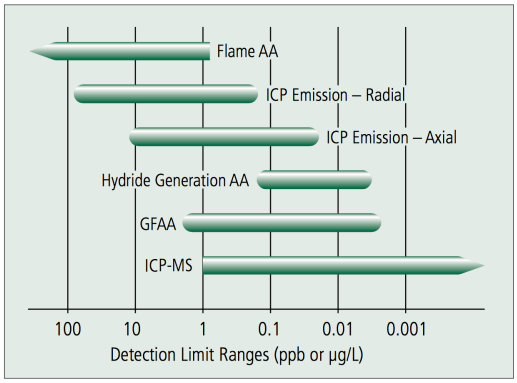

Figure 5.2: Typical detection limit ranges for the major atomic spectroscopy techniques. Adapted from [PerkinElmer, 2009].

All irradiations were performed on the IBA Cyclone 18/9 HC cyclotron present at ICNAS (Figure 5.3), capable of accelerating protons up to 18 MeV and deuterons up to 9 MeV.

Figure 5.3: Cyclone 18/9 MeV from IBA.

Most cyclotrons have a fixed energy beam (in our case, 18MeV). For the production of ^{68}Ga, we need to optimise that energy so as to minimise the production of ^{67}Ga. As presented in section 4.3, the threshold for $^{68}\mathrm{Zn}(p,2n)^{67}\mathrm{Ga}$ is 12.16MeV, so a good compromise between maximum production of ^{68}Ga and minimum production of ^{67}Ga can be achieved at energies close to 12MeV. The easiest way to decrease the energy of the beam is to pass it through an energy degrader in the form of a foil or a plate [Siikanen et al., 2014].

Targetry selection is a crucial step in cyclotron production of radionuclides [Skliarova et al., 2015]. The adequate material for both the target body and foil window depends on the nuclide production process being studied and possible corrosion, activation and cooling of the target bodies have to be considered [Bechtold et al., 1989].

For the production of ^{68}Ga a zinc nitrate ($^{68}\mathrm{Zn}(\mathrm{NO_3})_2$) solution was bombarded in a Niobium body target with a 250μm niobium window foil, cooled by water and helium. As mentioned, this thickness degrades the proton beam to suitable reaction energies and also lowers the risk of foil breaks and consequent damage to the cyclotron. Niobium was selected for its excellent chemical inertness, good thermal conductivity and high melting point [IAEA, 2012].

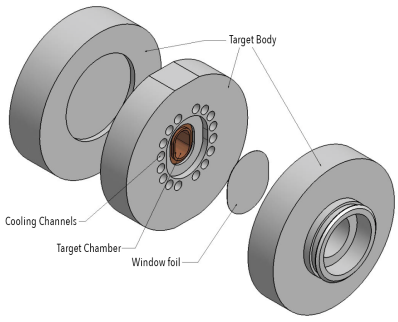

Figure 5.4: Schematic of the main liquid target components [Stokely, 2008].

Furthermore, an Agilent 1200 series HPLC system (Agilent Technologies, USA) equipped with a multi wavelength UV detector and a GABIStar NaI(Tl) radiometric detector (Raytest Isotopenmessgeraete GmbH, Strauben-

hardt, Germany), installed at ICNAS, was used to run chromatographic analysis and determine the radiochemical purity of the [^{68}Ga]DOTA-NOC produced.

5.2 Samples and Reagents

Nitric acid (HNO_3) (1-5 %) matrices are commonly used for sample dilution and as blank solution [Thomas, 2004]. This preference is related to the metal dissolution properties of HNO_3 and the fewer interferences it reads, as compared to other acids [Gaines, 2011].
All samples were diluted with a solution of 2% HNO_3 prepared from 69.2% HNO_3, purified using a subPur sub-boiling distillation set-up (Milestone Inc.), and from Water CHROMASOLV Plus grade.

Before each use, a fine tuning of the instrumental parameters, as well as a mass calibration, of the ICP-MS should be performed, so as to optimise the sensitivity of the instrument and to verify that the mass resolution meets the required specifications. Such procedure can be performed in a somewhat automated way, called "autotune". The number of instrumental parameters that can be optimised is large (> 30) and these parameters are correlated, so the tuning procedure is a non-linear optimisation process that, hopefully, will converge to the optimum setting for a given specification of the required performance - sensitivity, stability and oxide/double charge species ratio. The idea is to maximise the sensitivity (intensity/concentration), ensure the stability (repeated measurements should agree within specified RSDs) and minimise, at the same time, the amount of oxide and doubly charged species. The latter can be reduced at the expense of sensitivity acting on the extraction lenses voltages and by reducing the temperature of the plasma. The collision cell voltages should be optimised. The "autotune" is a time consuming process, especially if the ICP-MS is not operated regularly and the starting setting points are far from the optimum point. The order of the optimisations steps is important, mainly in the first cycles. One typically should start be optimising the parameters of the sample introduction system

and the torch position in x, y and z in order to get a sensible starting intensity at the detector (Figure 5.5). Then one proceeds with the tune of the extraction lenses and collision cell voltages. Naturally, these are different if one uses this cell merely as a focusing device or as a KED filter with He (or other) gas.

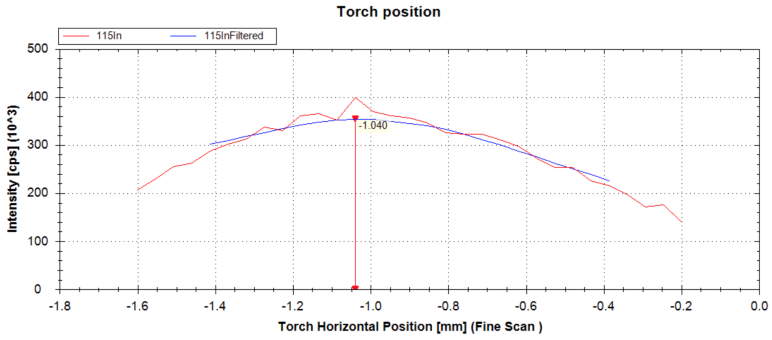

Figure 5.5: Tune Data View Source Autotune wizard showing the optimisation of the torch position.

Mass calibration is checked by default in the "autotune" procedure, but it is quite stable and seldom a full mass calibration, in which case the parameters of the quadrupole analyser are changed) is needed. However, the user can specify whether the instrument should run in a higher resolution mode (mass with ~ 0.3 amu) or in a more stable, standard, intermediate resolution mode (mass width ~ 0.7 amu). In this work we used the standard mass resolution (Figure 5.6).

The "autotune" uses a (multi-element) "tuning" solution. This solution contains analytes which are representative of the entire mass range capable of being scanned by the instrument: Li, Co, In, Ba, Bi, Ce and U. Ba is used mainly for checking the presence of doubly charged ions, whereas Ce is used for detection of oxides. The tuning solution used in all experiments was the Tune B ICAP Thermo Standard (500 mL), a certified reference material set in a HNO_3/HCl matrix.

All samples analysed in this project were involved in the cyclotron production of [^{68}Ga]DOTA-NOC, including reagents (like acetone or HCl) and eluates from the various steps of the process schematised in Figure 5.8.

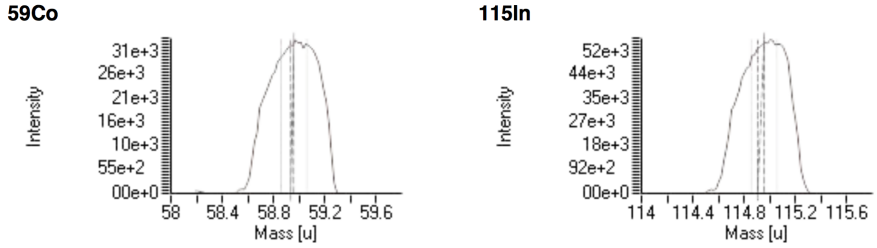

Figure 5.6: Example of the mass spectra at the ^{59}Co and ^{115}In peaks.

5.3 Standards

Standards are used in ICP-MS for accurate quantification of individual elements present in a sample. Since there is a linear relation between the intensity of the ion signals and the concentration of an element [Thomas, 2004], by using standard solutions we can generate calibration curves for specific elements. Therefore, to establish the concentration of a given element, the counts measured for that element are plotted against the calibration curve.

The following standards were acquired from Sigma-Aldrich:

- Multi-element standard solution 4 for ICP, TraceCERT (Fig. 5.5), in 10 % nitric acid (ref. 51844). Its composition is specified in Table 5.3.
- Niobium Standard for ICP, TraceCERT, 1000 mg/L Nb in nitric acid (ref. 67913)
- Tantalum Standard for ICP, TraceCERT, 1000 mg/L Ta in nitric acid and hydrofluoric acid (ref. 16641)
- Tungsten Standard for ICP, TraceCERT, 1000 mg/L W in nitric acid and hydrofluoric acid (ref. 50334)

Analogous to sample preparation, all standards were diluted using a 2% HNO_3 solution. The dilutions take in consideration the range of analyte concentrations anticipated in samples. For the multi-element standard a dilution factor of 2000 was used; for niobium a factor of 20000; and for tantalum and tungsten a factor of 40000. It should be noted that these dilutions had

Figure 5.7: Example of the standards used in this project. The image depicts the Multi-element (17 elements) Standard from Sigma-Aldrich.

Element	Concentration (mg/L)
Al	40
As	40
B	100
Ba	40
Be	10
Cd	10
Co	10
Cr	20
Cu	20
Fe	100
Mn	10
Ni	20
Pb	40
Se	100
Tl	100
V	40
Zn	100

Table 5.3: Composition of the multi-element standard used.

to be performed very carefully because linearity of the calibration curve is extremely important for accurate results.

5.4 Method for ^{68}Ga-DOTA-NOC production

The cyclotron production of ^{68}Ga starts with the irradiation of a 1.7M solution of isotopically enriched zinc nitrate ($^{68}Zn(NO_3)_2$) hexahidrate. Several experiments were performed for different irradiation times and with a target beam current of 27μA.

[^{68}Ga]DOTA-NOC was prepared using an automated synthesis module. The major steps of the production are schematised in Figure 5.8.

After irradiation, the target dump was collected and diluted ($\times$10). That solution was then passed through a strong cation exchange column (SCX - DOWEX 50WX8 hydrogen form, from Sigma-Aldrich) where $^{68}Ga^{+3}$ and

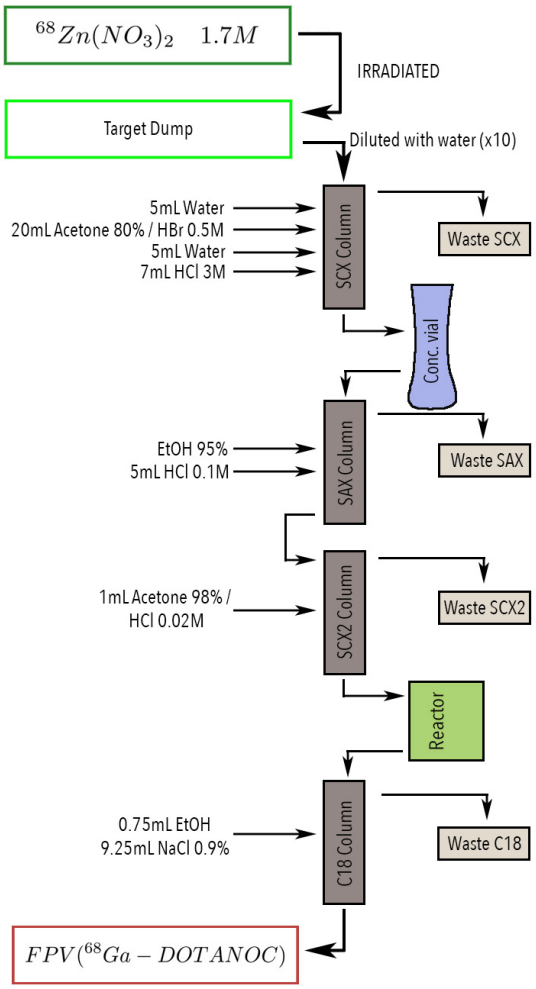

Figure 5.8: [^{68}Ga]DOTA-NOC preparation route.

$^{68}Zn^{+3}$ were trapped. This column is rinsed with 5mL of water to remove unwanted species such as ^{11}C and ^{13}N isotopes. Afterwards, 20mL of HBr 0.5M in 80% acetone solution were passed through the column to elute $^{68}Zn^{+3}$, which is recovered for future conversion to ($^{68}Zn(NO_3)_2$). Another 5mL of water were used to ensure that any remains of Ac80%/HBr0.5M were washed out. And finally, $^{68}Ga^{+3}$ was converted into $[GaCl_4]^-$ and eluted from the SCX column with 7mL of HCl 3M and collected in a concentration vial. These steps are crucial, an efficient separation of $^{68}Ga^{+3}$ is important to achieve good results at the end.

The following steps involve a purification of the eluate using a strong anion exchange column (SAX - AG 1-X8 Resin, acetate form, from Bio-Rad). A prior concentration of the eluate with HCl 12.6M is performed. The highly concentrated HCl complexes with ^{68}Ga making adsorption to the SAX column possible. This column was then washed with 95%EtOH and the ^{68}Ga, afterwards, extracted with 5mL of HCl 0.1 M. The SAX column purifies the gallium solution but leaves it with a very low pH which prevents the reaction with the DOTA-NOC peptide in the reactor. To avoid this, a second SCX column was used. The solution was then eluted from this column to the reactor with a 98% acetone/ HCl 0.02 M solution. In the reactor ^{68}Ga was mixed with the DOTA-NOC peptide in a buffer solution and heated.

By the end of the labelling reaction the solution was purified using a ^{18}C cartridge which retains [^{68}Ga]DOTA-NOC and releases unchelated $^{68}Ga^{+3}$ and acetone. At last, 0.75mL of EtOH were used to extract the peptide and 9.25mL of NaCl 0.9 % were added to dilute the solution.

Chapter 6

Results and Discussion

High specific activity radiopharmaceuticals are needed in order to properly image certain parts of the body, such as the brain. To produce high specific activity ^{68}Ga radiopharmaceuticals, the eluates must have high activity concentrations and also be relatively clean of contaminations from metals, otherwise the specific activity will not be sufficient.

Take as an example Figure 6.1, a chromatographic analysis . It shows that a great amount (70.39%) of unchelated $^{68}Ga^{3+}$ is found in the final product solution obtained at ICNAS, which is far from ideal. Clearly, the labelling efficiency was compromised, most likely because of metal ion contamination.

Metal ion contamination can interfere with $^{68}Ga^{3+}$ chelate binding, by substituting $^{68}Ga^{3+}$ with other metals. This is possible because a good part of the chelates currently used, form stable complexes with other metal ions. Iron, zinc, aluminium and copper are some of the metals that have high impact on the labelling efficiency of ^{68}Ga. These contaminants need to be accounted for and reduced or removed if possible.

Generator produced ^{68}Ga is relatively well studied, and so we expect Fe^{3+} and Zn^{2+} to be the most probable contaminants during a cyclotron based production. It was still necessary to identify where exactly the problem originated and also look for other potential sources of contamination,

inherent to the cyclotron production. Such candidates for contaminants as Tantalum and Tungsten − elements present in the cathodes −, or Niobium − from the target − are to be investigated.

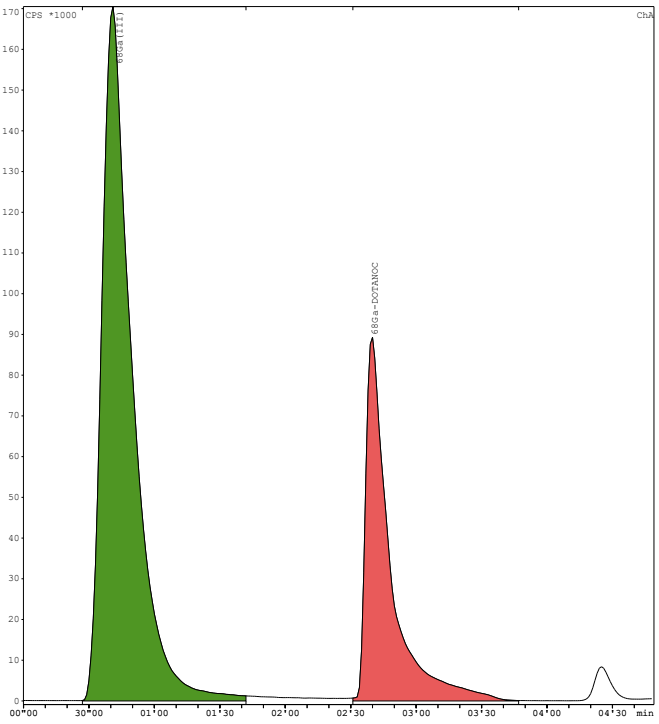

Figure 6.1: HPLC chromatogram of a final solution of [^{68}Ga]DOTA-NOC before any adjustments were made to the production. The green peak corresponds to the unchelated (free in the solution) $^{68}Ga^{3+}$. The red peak is the ^{68}Ga-DOTA-NOC. From the integral of the curve, the HPLC technique determined that 70.39% is free $^{68}Ga^{3+}$ and only 29.61% corresponds to the labelled peptide.

In this work, ICP-MS was used to analyse our samples and identify any possible contaminant elements and in which part of the process they were introduced.

Figure 6.2 shows an example of the information we can get from ICP-MS. In it we can visualise the calibration curve obtained through the measurements of the standards and the blank solution (ultra pure water with 2% ultra pure HNO_3). As mentioned before in Table 5.3, the standards used are cer-

tified standards traceable in composition and concentration to international standards at NIST.

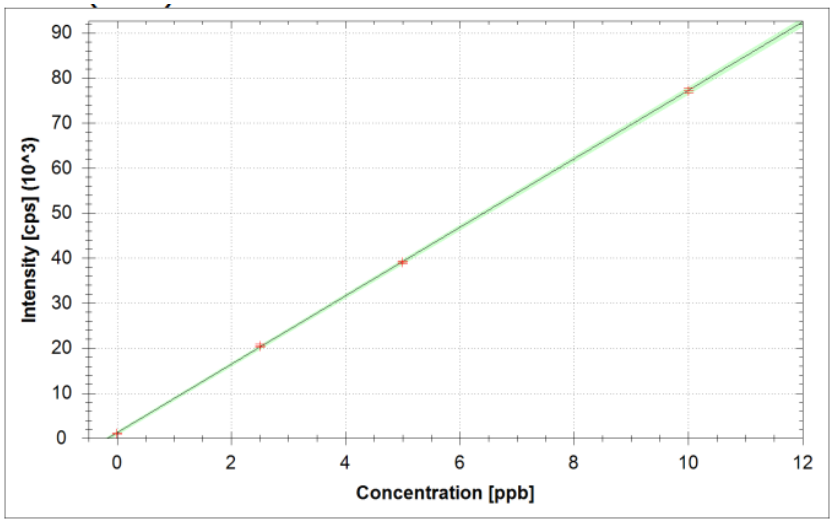

Figure 6.2: Example of a calibration curve. Calibration curve for isotope ^{60}Ni in He KED mode at 2.5, 5 and 10 ppb. The equation for the curve is given by $f(x) = 7603.2420 * x + 1217.5317$, with a correlation of $r^2 = 1.000$. BEC = 0.160 ppb and LOD = 0.0201 ppb.

When computing the calibration curves, enough points need to be calculated with the standards in order to properly characterise the response function. At least three values of standard concentration are recommended. Ideally, one with very low concentration, one at the high concentration limit expected for the samples and the rest spread out evenly across the calibration range.

Using the standards, we can dilute them the number of times needed to have a range of concentration covering the desired values. ICP-MS response is a highly linear function of concentration so we decided it would be enough to use just three different concentration values for our calibration: the standard with a specific dilution (see subchapter 5.3), 50% of that and 25% of that, along with the blank. These concentrations were chosen to cover the 100 ppb range, typically.

These points are then fitted to a linear regression curve ($I = f(x) = bx+a$, I = intensity, x = concentration). The iCAP-Q software allows us to choose

between forcing the calibration curve through zero ($f(0) = 0$), the blank measurement ($f(0)$ =blank intensity), or no forcing at all. We opted for not forcing the fit so as to have a clear insight about the blank quality.

ICP-MS relies fully on these calibration curves to compute the analyte concentration of the samples, by inverting the linear relation between intensity and concentration: $x = f^{-1}(I)$. The extrapolation of the linear calibration curve to $x = 0$, that,ideally, should coincide with the measurement of the blank solution ($x = 0$), gives us an idea of the contamination of the blank for that particular analyte. This blank intensity should be as low as possible because, ultimately, the blank quality will determine the lowest concentration that can be measured in the ICP-MS experiment. A low count rate of the blank ensures that both water, nitric acid and the instrument are clean.

Lower blank counts, which means lower contamination, provide better detection limits. The limit of detection (LOD), also known as instrument detection limit (IDL), can be defined as,

$$\text{LOD} = \frac{3 \times \text{STD of blank intensity} \times \text{sample concentration}}{\text{sample intensity} - \text{blank intensity}}, \tag{6.1}$$

where STD means the standard deviation.

The LOD can be interpreted as a measure for several factors, including the sensitivity of specific isotopes and also the background equivalent concentration (BEC). This last factor varies according to the purity of the reagents and water used by the equation:

$$\text{BEC} = \frac{\text{blank intensity} \times \text{standard concentration}}{\text{standard intensity} - \text{average blank intensity}}. \tag{6.2}$$

By controlling these variables, as much as possible, to keep the LOD down, it makes it easier to separate an analyte signal from the background.

Note that the BEC depends only on the blank intensity (for a given calibration). A high BEC means that the blank has already many counts for that analyte. However, if this BEC is stable and can be measured with a low STD, one can detect an analyte above the BEC, provided the acquisition

time is long enough to get good counting statistics. In addition, one demands that all calibration points fit precisely on the linear calibration line. This is the idea behind the LOD. The LOD is not determined by the blank intensity but by the standard deviation of the blank.

Keep in mind that purity of the blank and the cleanliness of the environment limit the BEC, but the LOD is determined mainly by the stability of the instrument and the quality of the dilutions procedures. Ideally, in normal operating conditions, one should expect a BEC lower than 1 ppb and a LOD below 0.1 ppb.

At the start of this project, unfortunately, some mistakes were made that affected the quality of the initial results of our analysis. The first problem that was identified, and corrected, was the result of using separate water sources for the standards and the samples. As explained in chapter 2 this procedure introduces a major source of error in ICP-MS.

Additionally, at some point we noticed that the sample introduction system was not working properly, in fact, the tube that introduced the samples into the ICP-MS appeared to be the source of another problem. The tube was too long and the uptake time, programmed by default in the instrument, was not enough for the sample to reach the plasma at a stable and steady rate. So the tube had to be shortened. When using the original long tube a big part of the sample was not reaching the detector in time and it was biasing our data. In fact, for each isotope, three consecutive measurements are taken by the instrument. The idea is to take the average and STD of the three measurements to use as actual data. One can see from Figure 6.3 that concentrations are increasing from the first to the third measurement, i.e. the count rate was increasing as the sample was arriving to the detector through the tube. By taking the average value shown as the horizontal line in Figure 6.3 as the "bad" representative value we are biasing the data to lower concentrations. Moreover, the STDs of these measurements are higher and far from the error associated with the counting statistics. By cutting the tube, approaching the sample racks to the ICP-MS and increasing the uptake time for all samples we succeeded in solving this major problem.

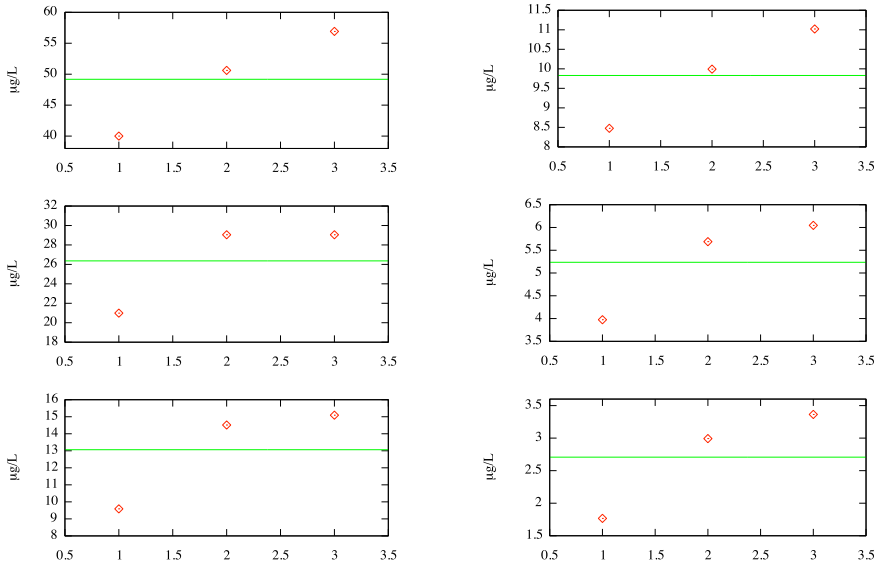

Figure 6.3: Example of delay in sample uptake for the 3 main runs performed for the standards of ^{57}Fe (a) and ^{53}Cr (b). Top line corresponds to initial dilution, middle line to 50% of that and bottom line 25%.

In an attempt to avoid both matrix and memory effects (high count rates that could damage the system) due to heavily charged solutions (mainly in Zinc), a precautionary approach was adopted. We opted for diluting by a large factor all samples that could potentially cause problems. This measure, however, resulted in occasional unreliable and unusable data of low count rates or give unreproducible results. So, the problem was: either we faced loss of information because the sample was too diluted or, if the sample wasn't diluted enough, we faced contamination from memory effects and inaccuracy in the quantification because the range was too broad. This problem ended up compromising the data for Zn in the samples, the results were unreliable and therefore are not included.

Sample analysis: iron

We present next the results obtained in the first runs of our samples, focusing the analysis on the iron isotopes, that could be a major contaminant. The four Fe isotopes have the natural abundances shown in Table (6.1). In this table we provide also the intensity measured on the ICP-MS working in KED mode for the most concentrated standard solution (a multi-element solution with 50 ppb of Fe). It is clear from the experimental data that the count rates measured for the 3 isotopes of lower mass agree with the natural abundances, within error bars (less than 5%) , but the intensity measured for the ^{58}Fe is abnormally high, in fact about 100 times higher than the count rate that would be expected for the low-abundance ^{58}Fe isotope. The reason for the excess count rate measured at this mass channel is clear: it is due, most certainly, to the ^{58}Ni isotope, that has a natural abundance of 68.0%. This severe isobaric interference cannot be removed by the collision cell, as it only works for polyatomic interferences. This point will be further developed ahead.

Isotope	Abundance (%)	Intensity (cps)	R(%)
^{54}Fe	5.8	45446	5.6
^{56}Fe	91.7	739883	-
^{57}Fe	2.11	18587	2.3
^{58}Fe	0.28	209059	26

Table 6.1: Isotope abundances for Fe and their respective count rates for the standard solution of concentration 50 ppb (in He KED mode). R is the normalised ratio $0.917/I(^{56}\mathrm{Fe})$, that should be similar to the natural abundances.

The calibration curves show that the BEC values for all four iron isotopes - ^{54}Fe, ^{56}Fe, ^{57}Fe and ^{58}Fe (Figures 6.4, 6.5, 6.6 and 6.7), are comparable and lower than 3.5 ppb. Indeed, the BECs are almost identical for the three isotopes of lower mass, even if they correspond to very different count rates due to their different isotope abundance. Clearly, ^{56}Fe being by far the most abundant in nature, is the preferable isotope for Fe quantification. However, when different isotopes are available, they can be used for consistency check of the analytical procedure. It should be stressed that the large difference

in the y scales of the four graphs, are simply related to the isotope abundance.

In each graph, the blue line indicates, for a particular sample, the calculated concentration of Fe for each of the isotopes. This concentration can be simply read from the interception of the blue line with the x axis, and it is a simple linear inversion of the measured count rate of the sample (interception of the blue line with the y axis), from the linear calibration fit. It is clear from the figures that there is a considerable amount of iron present in the sample analysed, of the order of 70 ppb.

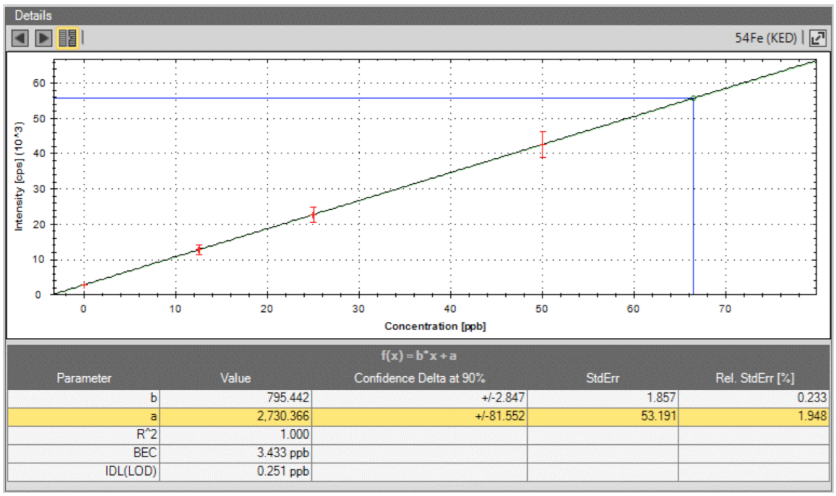

Parameter	Value	Confidence Delta at 90%	StdErr	Rel. StdErr [%]
b	795.442	+/-2.847	1.857	0.233
a	2,730.366	+/-81.552	53.191	1.948
R^2	1.000			
BEC	3.433 ppb			
IDL(LOD)	0.251 ppb			

Figure 6.4: Calibration curve for ^{54}Fe in He KED mode at 12.5, 25 and 50 ppb. The blue line indicates the concentration of ^{54}Fe for our sample - water used to pre-condition the SAX column.

Not surprisingly, the concentration estimated by the ^{58}Fe calibration curve gives a much different Fe concentration for the analysed sample. This value is clearly wrong; both the calibration points and possibly the analysed sample intensity at the ^{58}Fe channel are contaminated by the ^{58}Ni counts, and the calibration solution has a significant amount of Ni (12.5 ppb for the highest concentration point).

If one aims to use also the ^{58}Fe data (Figure 6.7) in the quantification of Fe, we need to take into consideration the isobaric interferences (section 2.1.6). We stress again that these interferences are due to an isotope of a

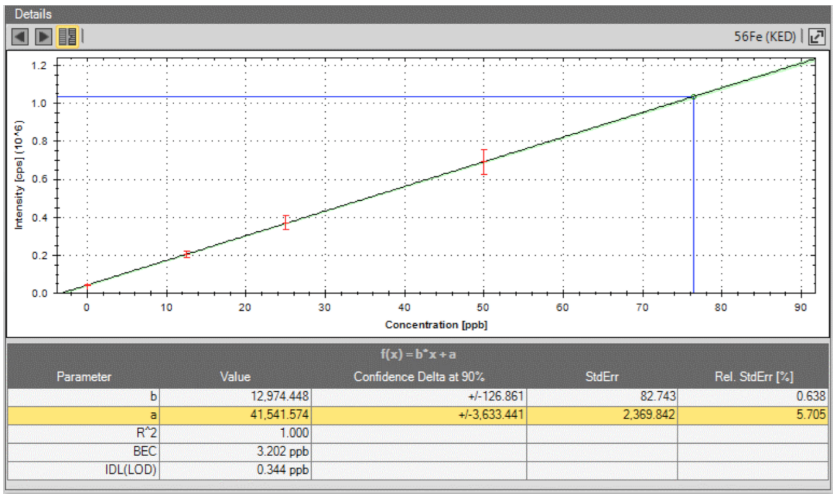

Parameter	Value	Confidence Delta at 90%	StdErr	Rel. StdErr [%]
b	12,974.448	+/-126.861	82.743	0.638
a	41,541.574	+/-3,633.441	2,369.842	5.705
R^2	1.000			
BEC	3.202 ppb			
IDL(LOD)	0.344 ppb			

Figure 6.5: Calibration curve for ^{56}Fe in He KED mode at 12.5, 25 and 50 ppb. The blue line indicates the concentration of ^{56}Fe for our sample - water used to pre-condition the SAX column.

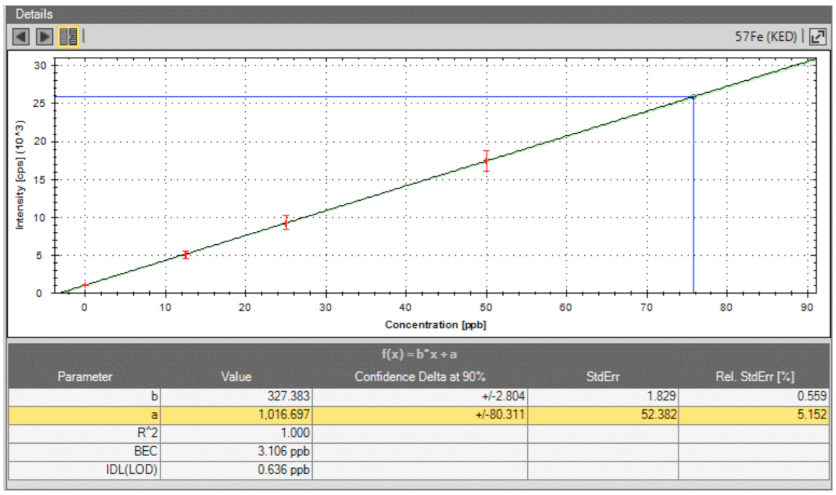

Parameter	Value	Confidence Delta at 90%	StdErr	Rel. StdErr [%]
b	327.383	+/-2.804	1.829	0.559
a	1,016.697	+/-80.311	52.382	5.152
R^2	1.000			
BEC	3.106 ppb			
IDL(LOD)	0.636 ppb			

Figure 6.6: Calibration curve for ^{57}Fe in He KED mode at 12.5, 25 and 50 ppb. The blue line indicates the concentration of ^{57}Fe for our sample - water used to pre-condition the SAX column.

different element than the analyte that has the same mass, ^{58}Ni in our case. ICP-MS cannot distinguish between the two isotopes as they sit in the same mass channel at the quadrupole analyser.

The interference in this case is very serious because of the low isotopic abundance of ^{58}Fe compared to that of ^{58}Ni. In fact, most counts at this

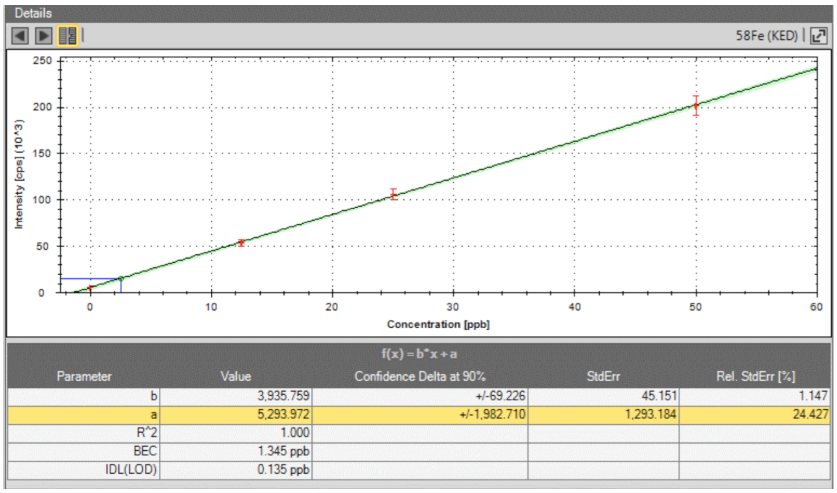

Parameter	Value	Confidence Delta at 90%	StdErr	Rel. StdErr [%]
b	3,935.759	+/-69.226	45.151	1.147
a	5,293.972	+/-1,982.710	1,293.184	24.427
R^2	1.000			
BEC	1.345 ppb			
IDL(LOD)	0.135 ppb			

Figure 6.7: Calibration curve for ^{58}Fe in He KED mode at 12.5, 25 and 50 ppb. The blue line indicates the concentration of ^{58}Fe for our sample - water used to pre-condition the SAX column.

channel are due to the Ni isotope, the contribution from Fe would be less than 1%. If we have good statistics and a very stable instrument, one could rely on subtracting the ^{58}Ni contribution estimated from the count rate measured at a different isotope using an appropriate interference correction equation[1]. Here, the isotope of choice would normally be ^{60}Ni, the second most abundant Ni isotope.

This interference correction is implemented in the software; yet it does limit the sensitivity, because ^{58}Ni is the most abundant isotope (68.077%) and we would be relying on a signal from a lower abundance isotope in the correction.

In our case, however, we came to the conclusion that could not make use of the interference correction equation. It continuously gave obviously wrong results. The equation overcorrected the Ni contribution, and the "clean" Fe count wold be negative. The only reason we envisage for such overcorrection would be either a different isotope abundance in the calibration solution from the natural one, which is very unlikely, or the ^{60}Ni channel is also contaminated with extra counts arising from some other interference. The most

[1]This correction subtracts from the ^{58}Fe count rate the count rate that is expected from the ^{58}Ni signal, based on the ^{60}Ni signal, as ($-2.61571\times$ ^{60}Ni).

likely interferences at the $m = 60$ channel are i) polyatomic ^{59}Co + H; ii) ^{40}Ar + ^{20}Ne. We do have a lot of Co in the multi-element standard solution, and Ar (certainly contaminated with other rare-gases) is ubiquitous in the system. These polyatomic interferences are tackled by the collision cell, but the small molecule of ^{59}Co + H will likely pass through to the analyser. In any case, if any of the two possible interferences are the cause of the problem, it could not be further corrected. A way to partially remove this problem would be to use a standard solution without Ni, so that the ^{58}Fe would be "clean". However, for the samples to be analysed, we cannot exclude a priori the existence of trace levels of Ni, therefore we conclude that the ^{58}Fe should not be used for Fe quantification, in any case. Fortunately, the other three isotopes of iron that are free from isobaric interferences are enough for a reliable quantification of this element.

The sample analysed in Figures 6.4, 6.5, 6.6 and 6.7 is the water used to pre-condition the SAX column (see Figure 5.8). This high amount of iron was not expected and this detection lead to a focused study in this part of the process in order to determine the problem and best course of action to solve or reduce it. The water used for the pre-condition was high-purity Chromasolv plus grade water, which is the same used for the dilutions. Since the problem seemed focused on the return from the SAX column, we can exclude the water itself as the source of contamination. This leaves two options, either the contamination is in the hydrochloric acid (HCl) used, or in the column itself.

It seemed more likely that the problem would be found in the reagent, because it is known that even very pure HCl contains a small quantity of Iron (Fe^{3+}), which even in the diluted solution used will give a measurable signal on the ICP-MS. It seems inevitable to have small amounts of Iron when using HCl in the process. In fact, HCl is so difficult to purify below ppb that this is one of the reasons why nitric acid is very much preferred as an acidic agent for preparing ICP-MS solutions.

In order to clarify these initial rough results, an analyse focused on the

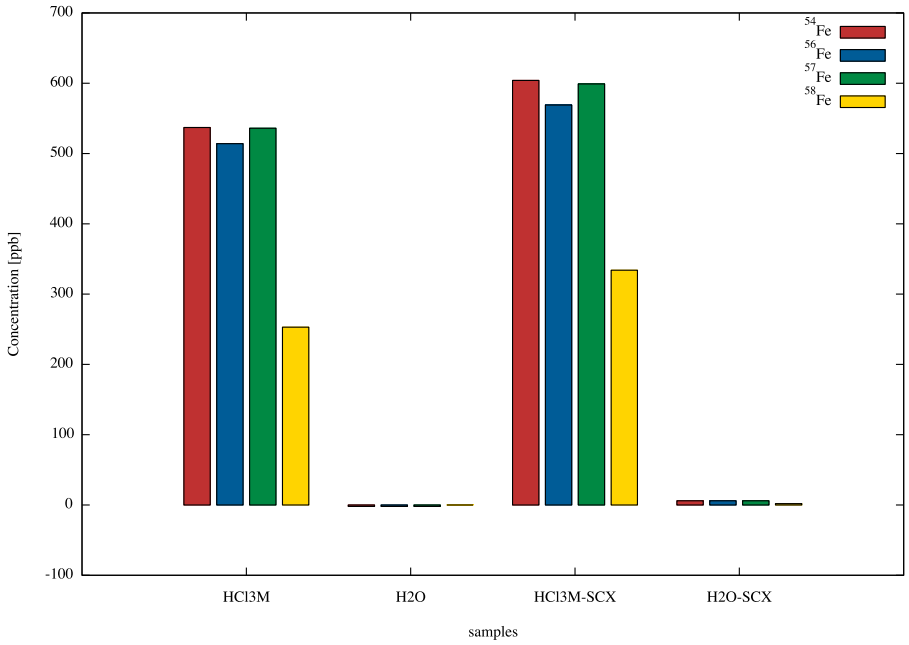

Figure 6.8: Comparison of Fe isotope concentration in HCl 3M and H_2O before and after passing through the SCX column.

exchange columns − SCX and SAX − and the reagents (HCl and ultra-pure water) used to pre-condition them was performed.

Figure 6.8 shows the concentration of iron determined by the ICP-MS for the pre-conditioning of the SCX column. The first sample represents a solution of HCl 3M (diluted $\times 100$). It's possible to see that it has a considerably high amount of iron (537 ± 16 ppb for the highest value [2]). That discovery was very important, because that reagent is used in several steps of the production. Looking at sample HCL3M-SCX - the HCl solution that was eluted through the column - we see that there's no apparent retention of iron from the SCX. The slightly higher amount of iron in this sample (604 ± 18 ppb for the same isotope) is not problematic, the calibration done for iron was based on standards with a maximum concentration of 50 ppb, so at higher values, a certain fluctuation is to be expected.

The second sample is water. The amount of iron measured is very low,

[2] For the previously presented interference reasons, we discarded the ^{58}Fe values as these were clearly unreliable

almost below the limit of detection achieved with the calibration. In comparison, sample H2O-SCX shows a small increase in iron concentration, possibly some residue of HCl left in the column, but not a significant amount.

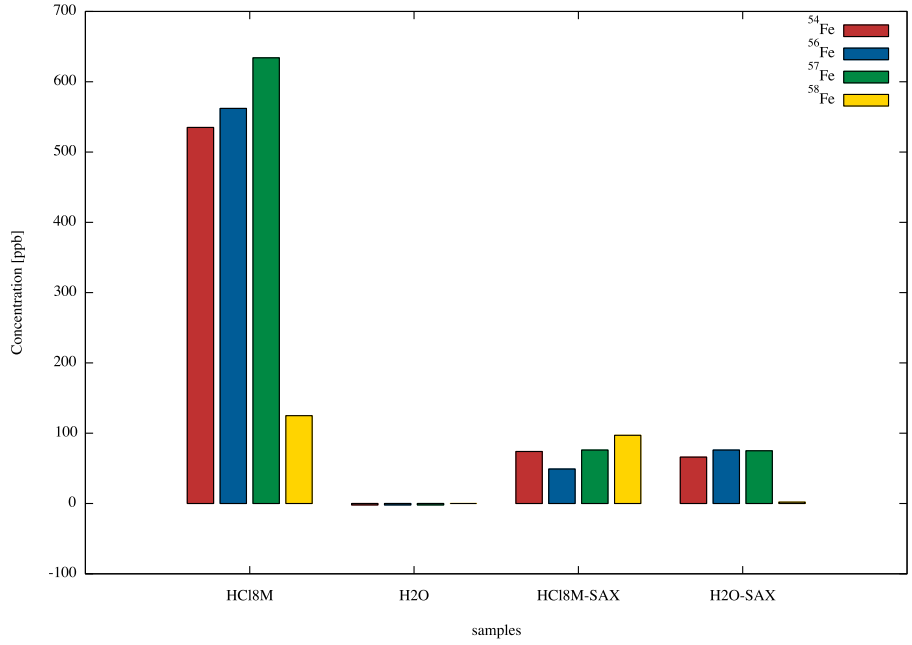

Figure 6.9: Comparison of Fe isotope concentration in HCl 8M and H_2O before and after passing through the SAX column.

For the SAX column (Figure 6.9), the same analysis was performed, comparing the HCl and water before and after elution. In this case, the HCl 8M (diluted x100) returned a similar result to the previously mentioned. However, the HCl eluate is dramatically different from what was expected. There's a clear retention of iron in the SAX column: a total of $83,98\%$ of iron. As shown in sample 4, the water used afterwards was not sufficient to completely wash off all the remaining iron in the column.

To be certain the problem was entirely in the HCl, a test was performed to rule out any contaminant build up in the SAX column resin. As can be seen in Figure 6.10, water was passed through the column several times to remove any remnants of contamination. Such water had no significant

Fe concentration, having count rates similar to the BEC or even below the BEC[3].Then, HCl went through the column (not shown in Figure 6.10) and finally the column was washed twice with 10 ml of water. In the first wash, the concentration of iron in the water was around 60 ppb, in the second it decreased to around 20 ppb. The iron build up in the SAX column seems to be entirely caused by the HCl.

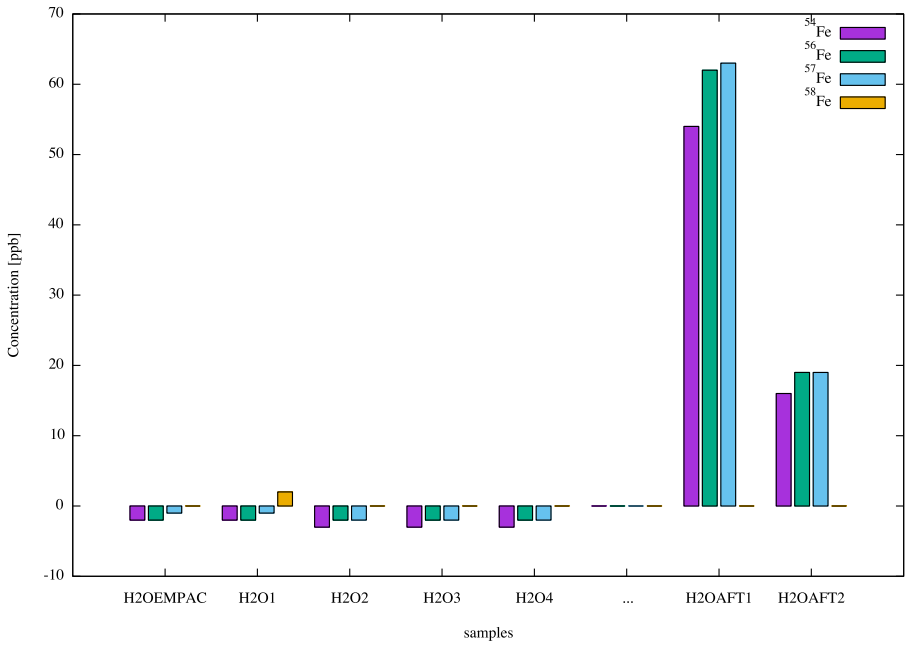

Figure 6.10: Comparison between samples of water fluted from the SAX column prior to and after passing the 8M HCl solution throught it.

Sample analysis: Aluminium, Tungsten, Tantalum and Niobium

Despite the high amount of iron detected, other sources of contamination were still pursued. We proposed to use the ICP-MS to conclude if Al^{3+}

[3]If the analyte count rate is below the BEC, the software will deliver a "negative" concentration; these, of course, have no other physical meaning rather than stating that the concentration of the analyte in the sample is of the order, or below, that of the ultra-pure water/HNO_3 2% used for the dilution of the standards. In any case, error bars, for such low count rates similar to background are typically high and "zero" is within the error bars.

influences the complexation of $^{68}Ga^{3+}$ with DOTA ligands. This was not possible due to the water that was at the time available having relatively high amounts of Al. Other studies concluded that the influence, in generator produced compounds, was very low, so no further study seemed necessary.

An initial study was performed to understand if either Tungsten, Tantalum or Niobium could be contaminants as part of some functional components have these metals present (e.g,ion source, target). In Table 6.2 and Figure 6.11 we can see results for Tantalum and Tungsten intensity in certain samples compared with the standards used and blank solutions.

Label	^{181}Ta Intensity (cps)	^{184}W Intensity (cps)
Standard setup	11865284	3058468
Standard 1/2	6284314	1578481
Standard 1/4	3104827	780680
Blank 1	1281	8187
Blank 2	1529	4582
Blank 3	2186	7663
Sample 1	3523	13950
Sample 2	2718	13306
Sample 3	1601	29131
Sample 4	581	5611
Sample 5	879	7180
Sample 6	1215	10187
Sample 7	563	8930
Sample 8	763	9905
Sample 9	513	8584
Sample 10	493	8387
Sample 11	496	12998
Sample 12	375	7704
Sample 13	1030	7727
Sample 14	855	10288
Sample 15	425	8346
Blank 4	1541	5291

Table 6.2: Intensities of ^{181}Ta and ^{184}W for various Standard dilutions, blanks and samples.

When we compare the values of all samples (apart from the standards),

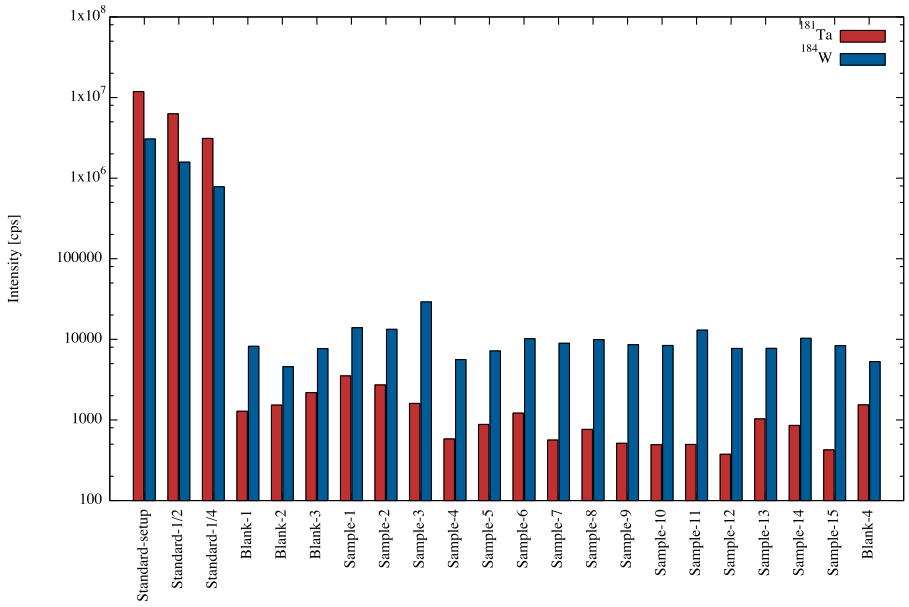

Figure 6.11: Intensity (represented in logarithmic scale) of ^{181}Ta and ^{184}W for various Standard dilutions, blanks and samples.

we see that the intensity values are quite similar, to a point where we can not say with any certainty if we have more tantalum present than the normal background amount. For that reason, and until further tests prove the contrary, we can say that the samples analysed appear to be free from tantalum and tungsten contamination.

For Niobium, the intensity counts were even lower than either tantalum and tungsten, reaching only a few hundred counts. This lead us to conclude that these three elements are not a major cause of contamination of the samples.

After these tests, only one major problem was identified, the contaminated HCl and the retention of iron in the elution of HCl through the SAX column.

The results indicate that there was a high contamination from iron in the HCl reagent and that was affecting the labelling of ^{68}Ga. It was decided to order a new traceselect HCl solution. And that a higher volume of water could be used in the pre-conditioning of the SAX column to ensure and remnants would be completely removed.

Figure 6.12 depicts an example of a chromatogram obtained after a successful production of DOTA-NOC. There's a radiochemical purity of 98.73% and the unchelated $^{68}Ga^{3+}$ is only 1.27%. This is a clear improvement from the initial results (Figure 6.1).

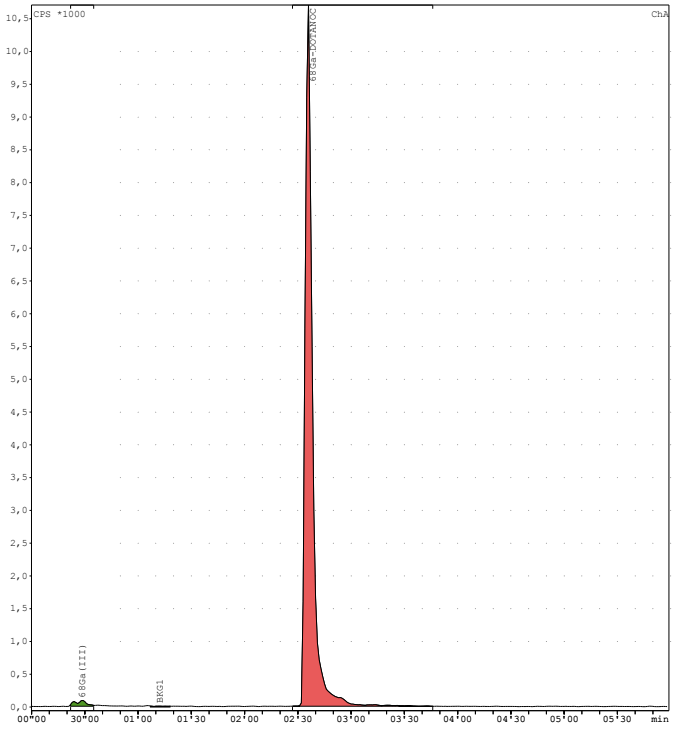

Figure 6.12: HPLC chromatogram of a final solution of [^{68}Ga]DOTA-NOC, after adjustments were made to the production. The green peak corresponds to the unchelated (free in the solution) $^{68}Ga^{3+}$. The red peak is the ^{68}Ga-DOTA-NOC. From the integral of the curve, the HPLC technique determined that only 1.27% is free $^{68}Ga^{3+}$ and 98.73% corresponds to the labelled peptide.

Chapter 7

Conclusions and Future perspective

The present work aimed to optimise the cyclotron production of ^{68}Ga for the development of the radiopharmaceutical [^{68}Ga]DOTA-NOC at ICNAS. A quantitative analysis of several samples from the method was performed using an ICP-MS. It was determined that the major contamination was coming from the HCl solution. This solution was used in a great number of steps in the process: from pre-conditioning of the anion/cation exchange columns, to the washing and eluting of ^{68}Ga from those same columns, as denoted in Figure 5.8.

While other factors (e.g., optimisation of the quantity of DOTA-peptide, or temperature, during the labelling step) may have been at play in the great change seen in incorporation of ^{68}Ga, understanding that a significant amount of iron was present in the HCl was key to improving the process. The obvious corrective measure we could take was buy a new solution with ultra-trace quality. Although it implied a greater expense, this greatly improved the radiolabelling process of the [^{68}Ga]DOTA-NOC and radiochemical purity $> 98\%$ is now obtained.

The biggest challenge that had to overcome during this project was the operation of the ICP-MS. It was a recent acquisition at the Physics Depart-

ment, and involved new techniques to be trained, as well as, specific details that could only be learned through experience. At first several mistakes were made but they were eventually identified and, when possible, corrected. Despite not having the best results, a simple solution was found and implemented through the work developed in this thesis, actively contributing to the optimisation of ^{68}Ga production method in an aqueous solution.

Had there been a higher budget or more "ICP-MS time", some revisions/improvements to the analysis could have been made and new experiments performed. For example, because of the high concentration of some elements in the samples, perhaps an acidified rinse (with the blank solution) should have been performed between samples, helping to clean the instrument. Another possibility could be running samples at two different dilutions to see how it affects the results. The demand for a big supply of Argon - analyses up to 30 or more samples at a time were being performed - prevented the elaboration of these tests.

Another aspect that stopped the flow of the project was the constant need to make new blank solutions (mostly because of water shortage). This introduced variables in the system making it impossible to compare samples in a timeline. Even more important perhaps is the quality of the water used for the blank solution, standards dilution and samples dilution. Traceselect water or Millipore water should have been use for all dilutions but the former is too expensive to be used in such quantities and we lacked the equipment for the latter. However, recently the Physics Department got access to a Millipore water purification system. In future work this equipment should be employed for obtaining the water.

Also, it should be noted that the recovery of the samples did not follow a methodic process. Meaning, the irradiation conditions varied, the samples we chose to analyse varied, as well as the steps in the method of production of DOTA-NOC.

The fact that we're dealing with radioactive samples also puts some constraints on the work: in order to avoid unnecessary exposure, we waited 2 to

3 days after the sample was recovered to analyse it. Such procedure is necessary because of ^{67}Ga, a contaminant, which has a half-life of 3.26 days. Some texts suggest that the ICP-MS analysis performed right after the production limits contamination.

One thing that could have been tried is the use of the ICP-MS collision cell using some gas appropriate for the isotope we wished to quantify. For instance, several studies report the use of ammonia to quantify iron. However, in this case a revision of the samples would have to be made, because with a collision cell we would have to take in consideration the high degree of specificity the use of a reactive gas would provide, as stated in studies from Edward McCurdy and Glenn Woods [McCurdy and Woods, 2004]. In other words, it would not be ideal for studies with a large range of analytes.

Future studies should include new analysis using Tungsten, Tantalum and Niobium standard solutions. The results obtained so far indicate that these elements are not the root cause of contamination. Still I suggest that a regular analysis should be performed to understand if over time these conditions change, meaning, if the ($^{68}Zn(NO_3)_2$) solution is causing corrosion of the Nb target and if the wear of the ion source is contaminating the solution.
Lastly, future experiments should also take in consideration the maintenance of the cyclotron: understand if changing the transfer lines reduces the amount of contaminants (it should because deposits of Zn and Fe, for example, can easily form), and if changing the ion source influences the amount of Ta and W found in the samples.

To summarise, this project and the ICP-MS technique were fundamental to identify a large contaminant in the method of production of 68Ga: iron. This information lead us to take an action to eliminate that contaminant and to, finally, achieve successful radiolabelling results for 68Ga-DOTA-NOC.

References

[Abrunhosa and Prata, 2008] Abrunhosa, A. and Prata, M. I. (2008). Radiofármacos: Desenvolvimento e Principais Aplicações. In J. P. de Lima, Editor, *Física em Medicina Nuclear*, Chapter 4. Imprensa da Universidade de Coimbra. p. xiv, 27, 38

[Agilent, 2010] Agilent (2010). *Collision/Reaction Cells in ICP-MS: Cell Design Considerations for Optimum Performance in Helium Mode with KED.* Agilent Technologies. p. 16

[Ahmad, 2013] Ahmad, M. (2013). Cyclotron Radionuclides for Health Care. Technical report, Pakistan Atomic Energy Commision. p. 22

[Ambrosini, 2014] Ambrosini, V. (2014). ^{68}Ga-DOTA-peptides in the diagnosis of NET. *PET Clinics.* p. 41

[Aslam et al., 2014] Aslam, M. N., Amjed, N., and Qaim, S. M. (2014). Evaluation of excitation functions of the ^{68,67,66}Zn(p,xn)^{68,67,66}Ga and ^{67}Zn(p,α)^{64}Cu reactions: Validation of evaluated data through comparison with experimental excitation functions of the ^{nat}Zn(p,x)^{66,67}Ga and ^{nat}Zn(p,x)^{64}Cu processes. *Applied Radiation and Isotopes.* p. 39

[Banerjee and Pomper, 2013] Banerjee, S. R. and Pomper, M. G. (2013). Clinical Applications of Gallium-68. *Applied Radiation and Isotopes.* p. 2, 35, 36, 42

[Bateman, 2012] Bateman, T. M. (2012). Advantages and disadvantages of PET and SPECT in a busy clinical. *Journal of Nuclear Cardiology.* p. 1

[Baum and Rösch, 2013] Baum, R. P. and Rösch, F., Editors (2013). *Theranostics, Gallium-68, and Other Radionuclides*, volume 194. Springer. p. 35

[Bazilio and Weinrich, 2012] Bazilio, A. and Weinrich, J. (2012). The Easy Guide to: Inductively Coupled Plasma-Mass Spectrometry (ICP-MS). p. xiii, 6

[Bechtold et al., 1989] Bechtold, V., Kernert, N., and Schweickert, H. (1989). Modern gas-target technology for the production of high quality radiopharmaceuticals. In *Proceedings of the 12th International Conference on Cyclotrons and their Applications: Berlin, Germany*. pp. 519–522. p. 46

[BiomonotoringMethods, 2012] BiomonotoringMethods (2012). The use of ICP-MS for human biomonitoring [Biomonitoring Methods, 1999]. In *The MAK-Collection for Occupational Health and Safety*. Wiley-VCH Verlag GmbH. p. 14

[Bronzino and Peterson, 2015] Bronzino, J. D. and Peterson, D. R., Editors (2015). *The Biomedical Engineering Handbook*. CRC Press, 4 edition. p. 28

[Brookhaven National Laboratory, 2012] Brookhaven National Laboratory (2012). Brookhaven Lab Named Historic Chemical Landmark. *The Journal Nuclear Medicine*, volume 53(12). p. 29

[Caramelo et al., 2008] Caramelo, F. J., Guerreiro, C., Ferreira, N. C., and Crespo, P. (2008). Detectores de radiação e Produção de imagens. In J. P. de Lima, Editor, *Física em Medicina Nuclear*, Chapter 5. Imprensa da Universidade de Coimbra. p. 33

[Cartwright, 2005] Cartwright, A. J. (2005). *Analysis of pharmaceuticals and biomolecules using HPLC coupled to ICP-MS and ESI-MS*. Ph.D. thesis, University of Plymouth, School of Earth, Ocean and Environmental Sciences, Faculty of Science. p. 12

[Clark and Buckingham, 1975] Clark, J. C. and Buckingham, P. D. (1975). *Short-lived Radioactive Gases for Clinical Use*. Butterworths London and Boston. p. 1

[Dams et al., 1995] Dams, R. F. J., Goossens, J., and Moens, L. (1995). Spectral and non-spectral interferences in inductively coupled plasma mass-spectrometry. *Microchimica Acta*, volume 119(3-4). p. 12, 13

[Dash and Chakravarty, 2014] Dash, A. and Chakravarty, R. (2014). Pivotal role of separation chemistry in the development of radionuclide generators to meet clinical demands. *RSC Adv.*, volume 4(81):42779–42803. p. xiv, 26, 27, 28

[Eberlein and Lassmann, 2013] Eberlein, U. and Lassmann, M. (2013). Dosimetry of [^{68}Ga]-labeled compounds. *Applied Radiation and Isotopes*, volume 76. p. 35

[Fani et al., 2008] Fani, M., André, J. P., and Maecke, H. R. (2008). ^{68}Ga-PET: a powerful generator-based alternative to cyclotron-based PET radiopharmaceuticals. *Contrast Media Mol Imaging*. p. 36, 37

[Fowler and Ido, 2002] Fowler, J. S. and Ido, T. (2002). Initial and subsequent approach for the synthesis of ^{18}FDG. *Seminars in Nuclear Medicine*, volume 32(1):6–12. p. 29

[Gaines, 2011] Gaines, P. R. (2011). *ICP Operations Guide: A Guide for using ICP-OES and ICP-MS*. Inorganic Ventures. p. 47

[Green and Welch, 1989] Green, M. A. and Welch, M. J. (1989). Gallium radiopharmaceutical chemistry. *International Journal of Radiation Applications and Instrumentation. Part B. Nuclear Medecine and Biology*, volume 16(5). p. 36, 42

[Griffeth, 2005] Griffeth, L. K. (2005). Use of PET/CT scanning in cancer patients: technical and practical considerations. *Bayl Univ Med Cent*. p. 30, 31

[Hanson, 2001] Hanson, M. W. (2001). Scintigraphic Evaluation of Neuroendocrine Tumors. *Applied Radiology*. p. 41

[Higgins and Pomper, 2011] Higgins, L. J. and Pomper, M. G. (2011). The Evolution of Imaging in Cancer: Current State and Future Challenges. *Semin Oncol*. p. 2

[Houk et al., 1980] Houk, R. S., Fassel, V. A., Flesch, G. D., and Svec, H. J. (1980). Inductively Coupled Argon Plasma as an Ion Source for Mass Spectrometric Determination of Trace Elements. *Anal. Chem.* p. 8

[IAEA, 2010] IAEA (2010). Production and Supply of Molybdenum-99. In *Nuclear Technology Review 2010*. p. 28

[IAEA, 2012] IAEA (2012). Cyclotron produced radionuclides: operation and maintenance of gas and liquid targets. In *IAEA Radioisotopes and Radiopharmaceuticals*, No. 4. International Atomic Energy Agency (IAEA). p. 46

[Jensen and Clark, 2011] Jensen, M. and Clark, J. (2011). Direct production of Ga-68 from proton bombardment of concentrated aqueous solutions of [Zn-68] Zinc Chloride. In *The 13th International Workshop on Targetry and Target Chemistry Proceedings*. p. 2

[Khan et al., 2009] Khan, M. U., Khan, S., El-Refaie, S., Win, Z., Rubello, D., and Al-Nahhas, A. (2009). Clinical indications for Gallium-68 positron emission tomography imaging. *Journal of Cancer Surgery*. p. 35

[Kleeven, 2004] Kleeven, W. (2004). *Isochronous cyclotron and method of extraction of charged particles from such cyclotron*. Google Patents. US Patent 6,683,426. p. 25

[Kleeven and Zaremba, 2015] Kleeven, W. and Zaremba, S. (2015). Cyclotrons: magnetic design and beam dynamics. In *CERN Accelerator School: Accelerators for Medical Applications*. p. xiv, 24

[Koppenaal et al., 2004] Koppenaal, D. W., Eiden, G. C., and Barinaga, C. J. (2004). Collision and reaction cells in atomic mass spectrometry: development, status, and applications. *Journal of Analytical Atomic Spectrometry*. p. 15

[Landon, 2006] Landon, M. R. (2006). *The application of ICP-MS to high matrix samples such as those found in the ceramics industry*. Ph.D. thesis, Loughborough University. p. 10, 11, 13, 14, 17

[Maecke and André, 2007] Maecke, H. R. and André, J. P. (2007). ^{68}Ga-PET Radiopharmacy: A Generator-Based Alternative to ^{18}F-Radiopharmacy. *Ernst Schering Research Foundation Workshop*. p. xv, 39

[Mathias et al., 2015] Mathias, C. J., Green, M. A., and Fletcher, J. W. (2015). Clinical PET/CT Evaluation of Patients with Neuroendocrine Cancer: Experience with Expanded Access IND Production and Use of ^{68}Ga-DOTA-NOC. Poster Presentation. p. xv, 42

[May and Wiedmeyer, 1998] May, T. W. and Wiedmeyer, R. H. (1998). A Table of Polyatomic Interferences in ICP-MS. *Atomic Spectroscopy*, volume 19(5):150–155. p. 13

[McCurdy et al., 2001] McCurdy, E., Wilbur, S., Woods, G. D., and Potter, D. (2001). Moving to the next level: Sample introduction and plasma interface design for improved performance in ICP-MS. In G. Holland and S. D. Tanner, Editors, *Plasma Source Mass Spectrometry: The New Millenium*. p. 44

[McCurdy and Woods, 2004] McCurdy, E. and Woods, G. (2004). The application of collision/reaction cell inductively coupled plasma mass spectrometry to multi-element analysis in variable sample matrices, using He as a non-reactive cell gas. *Journal of Analytical Atomic Spectrometry*. p. 73

[McCurdy et al., 2006] McCurdy, E., Woods, G., and Potter, D. (2006). *Unmatched Removal of Spectral Interferences in ICP-MS Using the Agilent*

Octopole Reaction System with Helium Collision Mode - Application. Agilent Technologies. p. 15, 16

[Morgat et al., 2013] Morgat, C., Hindié, E., Mishra, A. K., Allard, M., and Fernandez, P. (2013). Gallium-68: Chemistry and Radiolabeled Peptides Exploring Different Oncogenic Pathways. *Cancer Biotherapy and Radiopharmaceuticals.* p. 37

[Mueller et al., 2016] Mueller, D., Breeman, W. A. P., Klette, I., Gottschaldt, M., Odparlik, A., Baehre, M., Tworowska, I., and Schultz, M. K. (2016). Radiolabeling of DOTA-like conjugated peptides with generator-produced ^{68}Ga and using NaCl-based cationic elution method. *Nat. Protocols*, volume 11(6):1057–1066. p. 38

[Pandey et al., 2014] Pandey, M. K., Byrne, J. F., Jiang, H., Packard, A. B., and DeGrado, T. R. (2014). Cyclotron production of ^{68}Ga via the ^{68}Zn(p,n)^{68}Ga reaction in aqueous solution. *Am J Nucl Med Mol Imaging.* p. 2

[PerkinElmer, 2009] PerkinElmer (2009). *Atomic Spectroscopy - A Guide to Selecting the Appropriate Technique and System.* PerkinElmer. p. xv, 44, 45

[Phillips, 1996] Phillips, D. R. (1996). Radionuclide Generator Systems for Nuclear Medecine. In *Correspondence Continuing Education Courses for Nuclear Pharmacists and Nuclear Medicine Professionals*, volume 5. University of New Mexico. p. 27

[Prata, 2012] Prata, M. I. M. (2012). Gallium-68: A New Trend in PET Radiopharmacy. *Current Radiopharmaceuticals.* p. 35, 36, 37, 38

[Qaim et al., 1976] Qaim, S. M., Stöcklin, G., and Weinreich, R. (1976). *Iodine-123 in Western Europe (Production, Application, Distribution).* JÜL-Conf.-20. p. 1

[Rahmim and Zaidi, 2008] Rahmim, A. and Zaidi, H. (2008). PET versus SPECT: strengths, limitations and challenges. *Nuclear Medicine Communications*. p. 2, 30

[Richter, 2003] Richter, R. (2003). *Clean Chemistry Techniques for the Modern Laboratory*. Milestone Press. p. 17, 18

[Roesch and Riss, 2010] Roesch, F. and Riss, P. J. (2010). The Renaissance of the 68Ge/68Ga Radionuclide Generator Initiates New Developments in 68Ga Radiopharmaceutical Chemistry. *Current Topics in Medicinal Chemistry*, volume 10(15). p. 37, 42

[Saha, 2004] Saha, G. B. (2004). *Basics of PET Imaging*. Springer. p. 30

[Saha, 2010] Saha, G. B. (2010). *Fundamentals of Nuclear Pharmacy*. Springer. p. 26, 32

[Schubiger et al., 2007] Schubiger, P. A., Lehmann, L., and Friebe, M. (2007). PET Chemistry - The Driving Force in Molecular Imaging. Technical report, Ernst Schering Research Foundation. p. 41

[Siikanen et al., 2014] Siikanen, J., Tran, T., Olsson, T., Strand, S.-E., and Sandell, A. (2014). A solid target system with remote handling of irradiated targets for pet cyclotrons. *Applied Radiation and Isotopes*, volume 94. p. 46

[Šimeček et al., 2012] Šimeček, J., Hermann, P., Wester, H.-J., and Notni, J. (2012). How is ^{68}Ga Labeling of Macrocyclic Chelators Influenced by Metal Ion Contaminants in ^{68}Ge/^{68}Ga Generator Eluates? *CHEMMEDCHEM*. p. 39

[Skliarova et al., 2015] Skliarova, H., Renzelli, M., Azzolini, O., de Felicis, D., Bemporad, E., Johnson, R. R., and Palmieri, V. (2015). Niobium–niobium oxide multilayered coatings for corrosion protection of proton-irradiated liquid water targets for [^{18}F] production. *Thin Solid Films*, volume 591:316–322. p. 46

[Sörensen, 2012] Sörensen, J. (2012). How does the patient benefit from Clinical PET? *Theranostics*. p. 2

[Steiner, 2002] Steiner, M. A. (2002). *PET–The History Behind the Technology*. Ph.D. thesis, University of Tennessee. p. 29

[Stokely, 2008] Stokely, M. H. (2008). *Deployment, testing and analysis of advanced thermosyphon target systems for production of aqueous fluorine-18 via oxygen-18(p,n)fluorine-18*. Ph.D. thesis, North Carolina State University. p. xv, 46

[Szelecsényi et al., 1998] Szelecsényi, F., Boothe, T. E., Takács, S., Tárkányi, F., and Tavano, E. (1998). Evaluated cross section and thick target yield data bases of Zn+p processes for practical applications. *Applied Radiation and Isotopes*, volume 49(8):1005–1032. p. 39

[Tel et al., 2011] Tel, E., Sahan, M., Aydin, A., Sahan, H., A.Ugur, F., and Kaplan, A. (2011). The newly calculations of production cross sections for some positron emitting and single photon emitting radioisotopes in proton cyclotrons. In *Radioisotopes - Applications in Physical Sciences*. In Tech, Available from: http://www.intechopen.com/books/radioisotopes-applications-in-physical-sciences/. p. xv, 39, 40

[ThermoScientific, 2013] ThermoScientific (2013). *iCAP Q Operating Manual*. Thermo Fisher Scientific. p. xiii, 10, 12, 18

[Thomas, 2001-2002] Thomas, R. (2001-2002). A Beginner's Guide to ICP-MS. *Spectroscopy*, volume 16-17. p. 11, 12

[Thomas, 2004] Thomas, R. (2004). *Practical Guide to ICP-MS*, volume 33. Marcel Dekker, Inc. p. xiii, xix, 3, 5, 6, 7, 8, 10, 11, 13, 14, 15, 16, 18, 47, 49

[Thomas, 2008] Thomas, R. (2008). Practical Guide to ICP-MS : A tutorial for beginners. 2nd Edition. In *Practical Spectroscopy Series*, volume 37. CRC Press. p. 8, 9

[Tyler, 2015] Tyler, G. (2015). ICP-OES, ICP-MS and AAS Techniques Compared (accessed 15 september 2015). p. xix, 44

[Vandecasteele and Block, 1993] Vandecasteele, C. and Block, C. B. (1993). *Modern Methods for Trace Element Determination*. John Wiley Sons. p. 6

[Velikyan, 2014] Velikyan, I. (2014). Prospective of ^{68}Ga-Radiopharmaceutical Development. *Theranostics*, volume 4(1):47–80. p. xv, 2, 33, 35, 36, 37, 38, 42

[Vértes et al., 2011] Vértes, A., Nagy, S., Klencsár, Z., Lovas, R. G., and Rösch, F., Editors (2011). *Handbook of Nuclear Chemistry*. Springer. p. 26, 32

[Virgolini et al., 2010] Virgolini, I., Ambrosini, V., Bomanji, J. B., Baum, R. P., Fanti, S., Gabriel, M., Papathanasiou, N. D., Pepe, G., Oyen, W., Cristoforo, C. D., and Chiti, A. (2010). Procedure guidelines for PET/CT tumour imaging with ^{68}Ga-DOTA-conjugated peptides: ^{68}Ga-DOTA-TOC,^{68}Ga-DOTA-NOC, ^{68}Ga-DOTA-TATE. *Eur J Nucl Med Mol Imaging*. p. 36

[Wernick and Aarsvold, 2004] Wernick, M. N. and Aarsvold, J. N. (2004). *Emission Tomography, The fundamentals of PET and SPECT*, Chapter 2 - Introduction to Emission Tomography. Academic Press, pp. 11–23. p. 1

[WHO, 2008] WHO (2008). Radiopharmaceuticals. In *The International Pharmacopoeia*. p. 21